Figure 1 ECG of the proband and family pedigree. ECG shows sinus rhythm (*A*) and AF (*B*). The QT and QTc intervals were 172 and 194 ms, respectively. (*C*) Family pedigree. Arrow indicates the proband; a filled symbol indicates clinically and genetically affected individual.

She was diagnosed with SQTS from these clinical features (i.e. a markedly shortened QT interval, paroxysmal AF, and VF inducibility).

The proband had a family history of perinatal death in her elder sister (*Figure 1C*), but her family did not undergo genetic investigation or further clinical evaluation with the exception of ECGs taken for her father, elder brother, and younger sister. Genetic investigations could not be carried out due to a lack of informed consent. The ECGs for the family members displayed normal QTc intervals (410, 430, and 390 ms, respectively; *Figure 1C*).

3.2 Genetic analysis

In this patient, we screened for candidate cardiac ion channel genes (*KCNQ1*, *KCNH2*, *KCNE1-3*, *KCNJ2*, *CACNA1C*, and *SCN5A*). As a result of the genetic analysis, we identified a novel heterozygous mutation, a single-base substitution at nucleotide 902 (c.902T>A) in the *KCNJ2* gene, resulting in an amino acid change from methionine to lysine at 301 in the Kir2.1 potassium channel (*Figure 2A*). Met-301 is located in the C-terminal cytoplasmic domain of the channel

(*Figure 2B*).[13] The amino acid at codon 301 (methionine) is highly conserved among different species (*Figure 2C*). Furthermore, this mutation was absent in 400 Japanese control alleles. We failed to identify mutations in any other candidate genes.

3.3 Cell surface expression of KCNJ2 mutants

In order to investigate whether the M301K mutations affect intracellular Kir2.1 trafficking, we introduced an HA epitope into the extracellular domain of KCNJ2, and examined the subcellular distribution of channels in transfected HEK 293 cells using confocal microscopy[10] (*Figure 2D*). *Figure 2D* illustrates the typical results of confocal imaging. HEK 293 cells were successfully transfected with either HA-*KCNJ2* WT, *KCNJ2* WT/HA-M301K, or HA-M301K (*Figure 2D*, upper panels). All types of HA-tagged Kir2.1 proteins exhibited red fluorescence at the plasma membrane (*Figure 2D*, middle and lower panels), indicating that both homo- and heterozygous mutant channels were trafficking-competent.
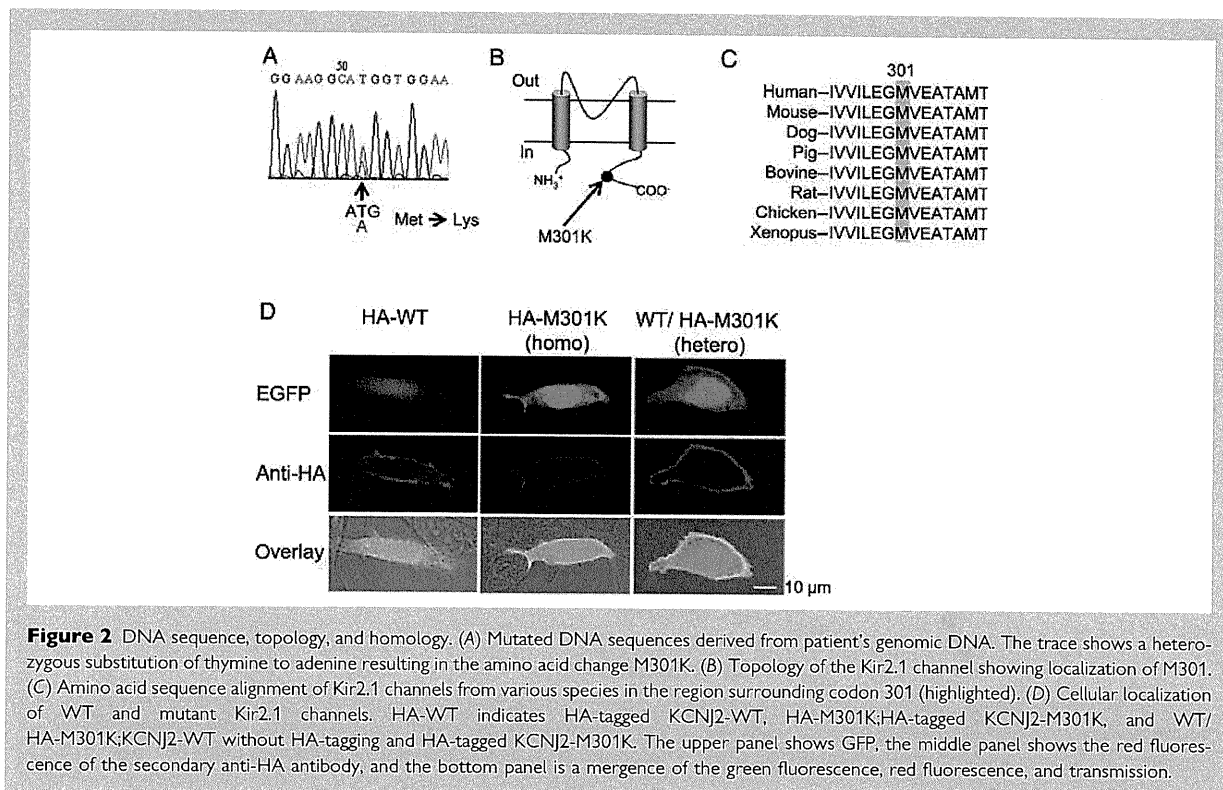
Figure 2 DNA sequence, topology, and homology. (*A*) Mutated DNA sequences derived from patient's genomic DNA. The trace shows a heterozygous substitution of thymine to adenine resulting in the amino acid change M301K. (*B*) Topology of the Kir2.1 channel showing localization of M301. (*C*) Amino acid sequence alignment of Kir2.1 channels from various species in the region surrounding codon 301 (highlighted). (*D*) Cellular localization of WT and mutant Kir2.1 channels. HA-WT indicates HA-tagged KCNJ2-WT, HA-M301K;HA-tagged KCNJ2-M301K, and WT/HA-M301K;KCNJ2-WT without HA-tagging and HA-tagged KCNJ2-M301K. The upper panel shows GFP, the middle panel shows the red fluorescence of the secondary anti-HA antibody, and the bottom panel is a mergence of the green fluorescence, red fluorescence, and transmission.

3.4 Cellular electrophysiology

We performed a functional characterization of the mutant channels in HEK 293 cells. *Figure 3A* shows representative current traces from cells expressing *KCNJ2* WT, M301K, or WT/M301K, elicited by voltage-clamp steps (duration 400 ms) from −120 to +100 mV (10 mV step), applied from a holding potential of −60 mV. The currents were normalized to cell capacitance and were plotted as a function of test potentials (*Figure 3B*). As previously reported, expression of the *KCNJ2* WT in HEK 293 cells resulted in normal inward rectifying potassium currents (*Figure 3A* left panel and blue symbols in *Figure 3B*). When M301K mutant channels were expressed alone, they were entirely non-functional (*Figure 3A* middle panel and green symbols in *Figure 3B*). In contrast, when cells were co-transfected with both equimolar WT and M301K, ample potassium currents showing a very weak inward rectification could be recorded (*Figure 3A* right panel and red symbols in *Figure 3B*). Average current densities were significantly smaller than those of WT Kir2.1 channels at potentials between −120 and −90 mV ($P < 0.05$), and significantly larger at potentials between −30 and +100 mV ($P < 0.05$).

3.5 Contribution of amino acid charge at residue 301 to Kir2.1 currents

Methionine at 301 is located within the G-loop that forms the narrowest segment of the cytoplasmic pathway,[13,14] and negatively charged amino acids on the inner wall of the cytoplasmic pore, where the G-loop is located, are known to be important for the strength of the inward rectification.[13–15] We therefore speculated

that the amino acid charge at this position may be crucial for the inward rectification of Kir2.1 channels, and that its change from methionine (neutrally charged) to lysine (positively charged) may result in functional changes in Kir2.1 currents. In order to analyse the contribution of the amino acid charge at 301 to inward rectification, we changed the amino acid at M301 to another positively charged amino acid, arginine, and to another neutral amino acid, alanine, for comparison. *Figure 4A* illustrates the whole-cell Kir2.1 currents in homo- and heterozygous mutant conditions for M301R (left panel) and M301A (right panel). Homozygous M301R mutant channels displayed no functional currents, whereas WT/M301R attenuated the inward rectification (*Figure 4A* left panel). These observations suggest that the currents through the M301R channels are similar to those of the M301K channels (*Figure 3*) under both homo- and heterozygous conditions. On the other hand, in the M301A channels—in which the residual charge remained neutral—the currents showed normal inward rectification in both homo- and heterozygous conditions similar to those produced by WT Kir2.1 channels (*Figure 4A* right panel). In order to evaluate the intensity of inward rectifying properties, we assessed the rectification index, along with the ratio of the current amplitudes at 0 and −100 mV.[15] *Figure 4B* shows the rectification indexes obtained from WT, M301A (0.10 ± 0.02, $n = 10$), WT/M301A (0.073 ± 0.015, $n = 11$), WT/M301K (1.12 ± 0.16, $n = 11$), and WT/M301R (0.99 ± 0.14, $n = 11$). Although the rectification indexes for WT/301A and M301A showed no significant difference, the indexes for both WT/M301K and WT/M301R were significantly increased in comparison with WT (0.061 ± 0.01, $n = 15$, $P < 0.001$, left-most bar in *Figure 4B*).
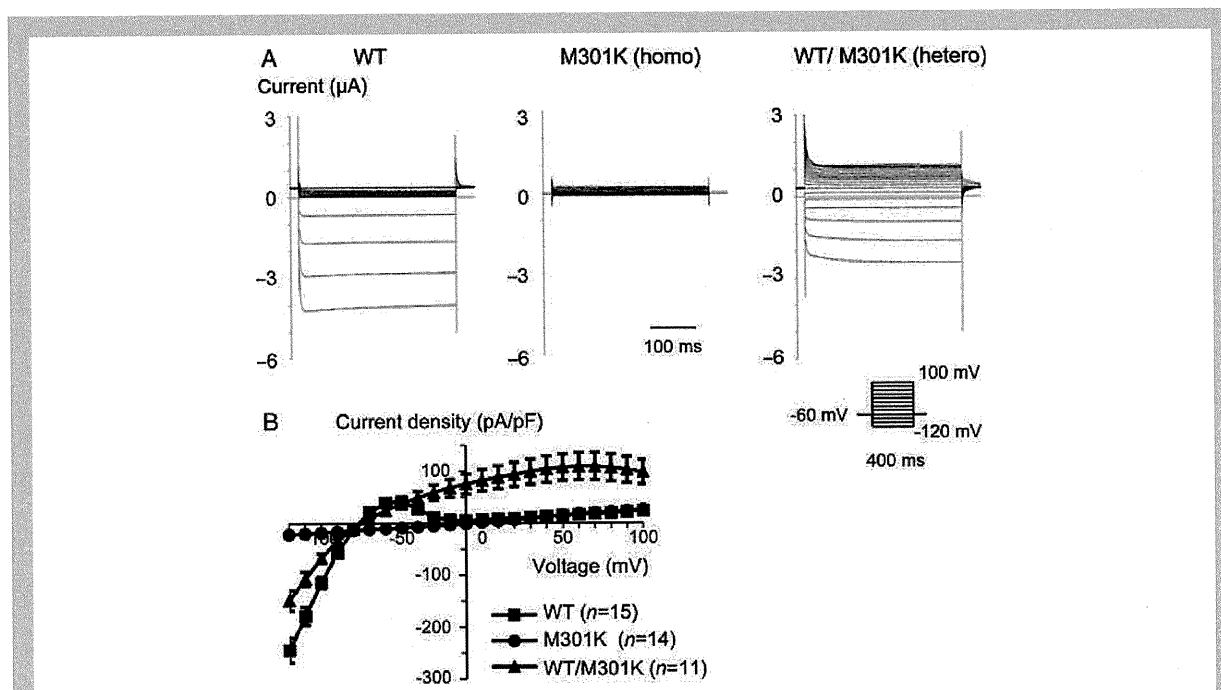
Figure 3 Voltage-clamp recordings from transfected HEK 293 cells. (A) Representative current traces of WT, M301K, and WT/M301K. Currents were elicited by 400 ms depolarizing voltage steps from −120 to +100 mV and from a holding potential of −60 mV. (B) Current–voltage relationships are plotted as the current. Current density was calculated by dividing the whole-cell current amplitude by cell capacitance. No functional currents were recorded in the homozygous M301K channels. On the other hand, the mean current densities of the WT/M301K channels are significantly larger than the WT (P < 0.05) at each voltage from −30 to +100 mV, and smaller at each voltage from −120 to −90 mV (P < 0.05).

3.6 Action potentials recording in *KCNJ2*-M301K-transfected NRVMs

We investigated the impacts of M301K mutant Kir2.1 channels on NRVMs' action potentials using a transient transfection method. *Figure 5A* shows typical action potentials recorded for non-transfected (control) NRVMs (*Figure 5A*, left panel), and NRVMs transfected with *KCNJ2* WT or WT/M301K (*Figure 5A* middle and right panels, respectively). Phase 3 repolarization was accelerated in the *KCNJ2* WT- and WT/M301K-overexpressed groups (*Figure 5A* middle and right panels, respectively) and we could further note that the dome is nearly lost in the WT/M301K group. APD$_{90}$ was significantly abbreviated in the *KCNJ2* WT-overexpressed group (28.2 ± 3.4 ms, $n = 10$, $P < 0.001$, *Figure 5A*, middle panel) in comparison with the control group (123.3 ± 12.2 ms, $n = 11$, *Figure 5A*, left panel; bar graphs in *Figure 5B*). Additionally, APD90 was significantly shorter in the WT/M301K mutant-overexpressed group (9.4 ± 2.1 ms, $n = 16$, $P < 0.001$, *Figure 5A*, right panel; bar graph in *Figure 5B*) than in the WT-overexpressed group.

4. Discussion

4.1 Major findings

In the present study, we identified a novel heterozygous *KCNJ2* mutation, M301K, in a patient with a markedly shortened QT interval. The QT interval, 172 ms, of this patient is the shortest among previous SQTS reports,[2–7,16] to our knowledge. The methionine at position

301 is located in the C-terminus of Kir2.1 channel, and is considered to form a pore-facing loop region.[13] Functional assays using a heterologous expression system revealed that homozygous M301K Kir2.1 channels carried no currents with preserved plasma membrane expression; however, heterozygous WT/M301K Kir2.1 channels attenuated inward rectifying properties, which resulted in increased outward currents for positive voltages and negative voltages down to −30 mV. Significant increases in outward currents within the voltage range of the action potentials shortened APD by accelerating membrane repolarization as shown in *Figure 5*, which is implicated in increased cardiac vulnerability.

4.2 Impaired inward rectification of Kir2.1 currents: a novel mechanism predisposing SQTS

In 2005, Priori *et al.*[4] first reported a heterozygous gain-of-function *KCNJ2* mutation, D172N, in a patient with SQTS. In the report, homozygous D172N Kir2.1 channels displayed larger outward currents compared with WT Kir2.1 alone, and heterozygous channels yielded intermediate results. In both homozygous and heterozygous D172N mutant channels, the inward rectification properties of Kir2.1 currents were preserved. In heterozygous M301K mutant channels identified in our patient, however, the inward rectification was significantly reduced, allowing ample outward potassium currents at positive potentials. In addition, it should be emphasized that the homozygous M301K mutant channels were non-functional. These functional changes, such as the impaired inward rectification of the
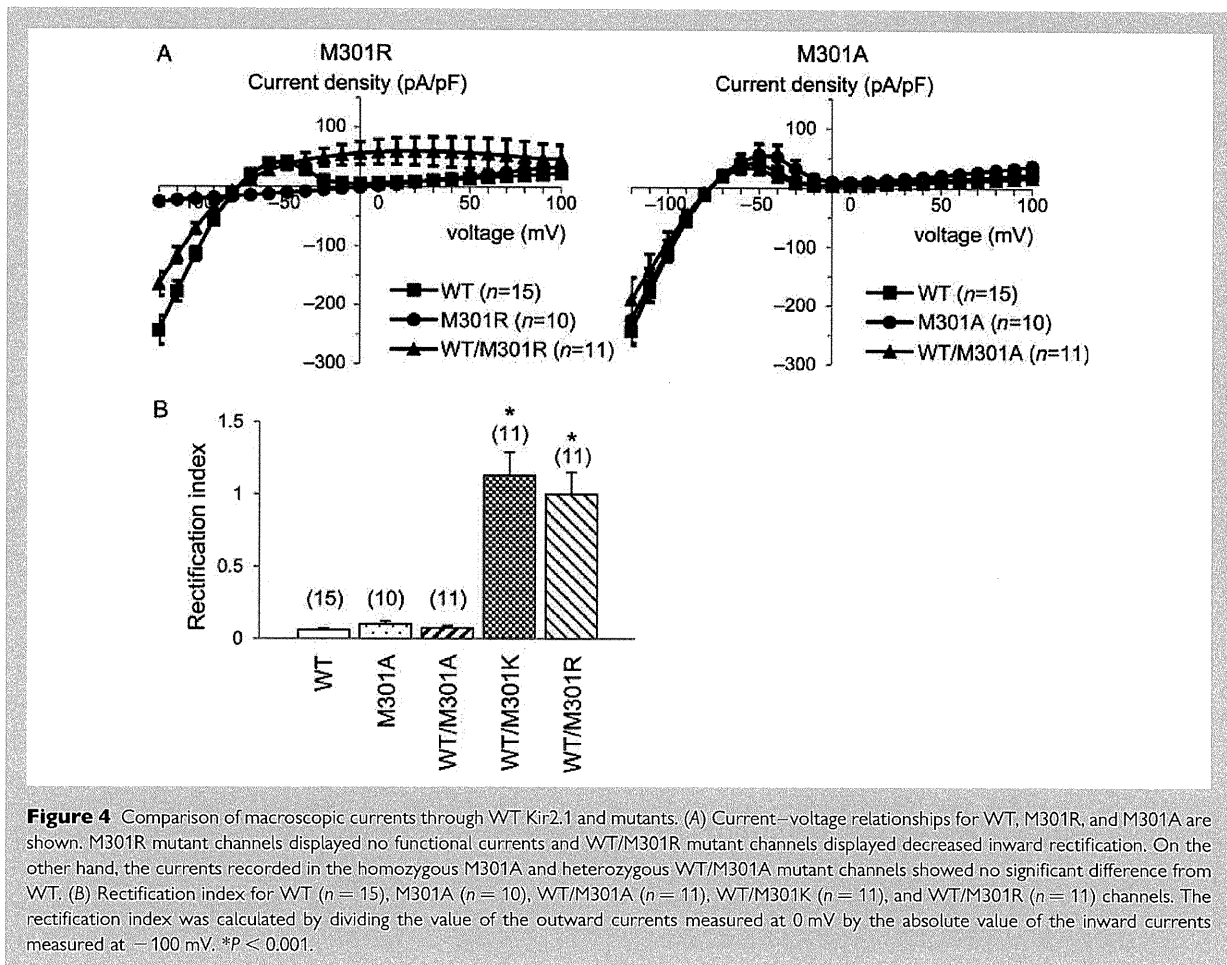
Figure 4 Comparison of macroscopic currents through WT Kir2.1 and mutants. (A) Current–voltage relationships for WT, M301R, and M301A are shown. M301R mutant channels displayed no functional currents and WT/M301R mutant channels displayed decreased inward rectification. On the other hand, the currents recorded in the homozygous M301A and heterozygous WT/M301A mutant channels showed no significant difference from WT. (B) Rectification index for WT ($n = 15$), M301A ($n = 10$), WT/M301A ($n = 11$), WT/M301K ($n = 11$), and WT/M301R ($n = 11$) channels. The rectification index was calculated by dividing the value of the outward currents measured at 0 mV by the absolute value of the inward currents measured at −100 mV. *$P < 0.001$.

Kir 2.1 currents resulting in increased outward currents, are a novel *KCNJ2* gain-of-function mechanism predisposing SQTS.

The phenotypic characteristics of our index patient somewhat differ from those of the *KCNJ2*-D172N mutation carriers.[4] No apparent arrhythmias were recorded with D172N mutation carriers. On the other hand, our M301K patient showed paroxysmal AF and multiple disorders. Additionally, mechanical stimulation by a Swan–Ganz catheter induced paroxysmal supraventricular tachycardia and VF. Moreover, the QTc interval in our patient was much shorter (QTc = 194 ms, *Figure 1*) than that of the D172N carriers (QTc = 315 and 320 ms).[4] Another gain-of-function *KCNJ2* mutation, V93I, was reported in a familial AF case.[17] Their functional analysis showed a similar result with D172N, but the affected members had normal QT intervals. These diverse clinical manifestations may be related to the extent and the different gain-of-function mechanisms of the Kir2.1 currents.

4.3 Relationship between impaired inward rectification and charged amino acid residues at 301

Kir currents exhibit strong inward rectification, which is thought to be due to pore blocking induced by multivalent ions from intracellular

Mg^{2+}.[18–20] Channel blockade by physiological concentrations of Mg^{2+} is influenced by the electrostatic negativity within the cytoplasmic pore.[15] Negative charges on the inner wall of the cytoplasmic pore are therefore key determinants of the strength of the inward rectification. Many amino acid residues inside the pore demonstrate interactions with the ion over long distances, suggesting that mutations potentially affect ion or blocker energetics over the entire pore profile.[14,21] The M301K mutation causes the change of the amino acid residue at 301 from a non-charged amino acid residue, methionine, to a positively charged residue, lysine. In order to evaluate the importance of the charge at 301, additional whole-cell patch-clamp recordings were carried out on M301A (remained neutral) and M301R (neutral to positive) (*Figure 4*). Inward rectification of Kir2.1 currents was well preserved in both homozygous and heterozygous M301A channels. Heterozygous M301R channels, however, attenuated inward rectification, and homozygous M301R channels were non-functional similar to that of the M301K channels. These electrophysiological results indicate that the neutral amino acid residue at 301 plays an important role in generating Kir2.1 inward rectification. The decrease in the net negative charge within the cytoplasmic pore may facilitate the reduction in both the susceptibility of the channel to Mg^{2+} block and the voltage dependence of the blockade. It
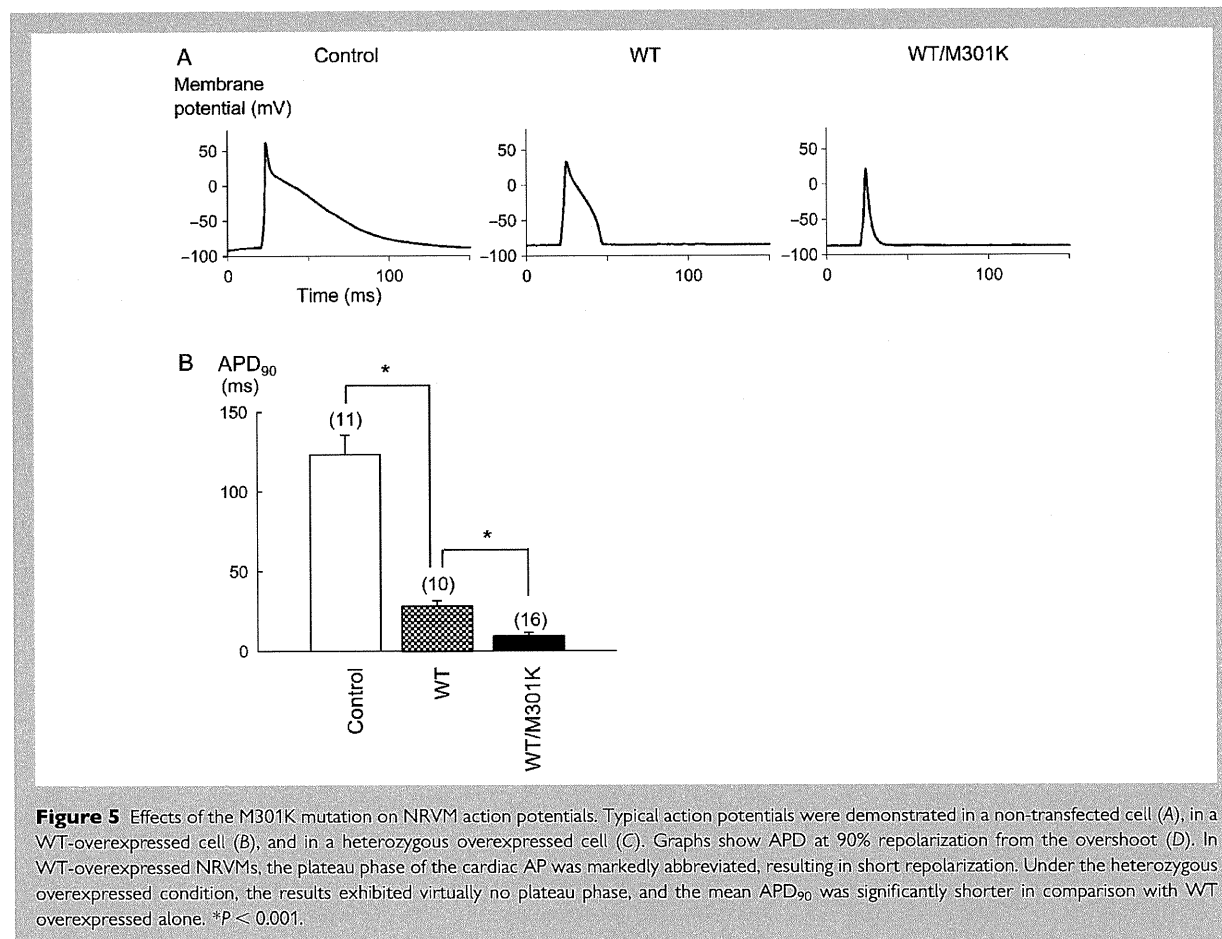
Figure 5 Effects of the M301K mutation on NRVM action potentials. Typical action potentials were demonstrated in a non-transfected cell (A), in a WT-overexpressed cell (B), and in a heterozygous overexpressed cell (C). Graphs show APD at 90% repolarization from the overshoot (D). In WT-overexpressed NRVMs, the plateau phase of the cardiac AP was markedly abbreviated, resulting in short repolarization. Under the heterozygous overexpressed condition, the results exhibited virtually no plateau phase, and the mean APD_{90} was significantly shorter in comparison with WT overexpressed alone. $*P < 0.001$.

remains unknown why only tentative hetero-multimers of WT and M301K are active and lose their inward rectification properties. In homozygous M301K channels, all of the tetrameric subunits must have a positively charged lysine at 301, which may impair potassium ion permeation due to a conformational change in the near-pore region.

4.4 Heterozygous *KCNJ2*-WT/M301K overexpression shortened APD in NRVMs

In cardiomyocytes, Kir2.1, Kir2.2, and Kir2.3 channels are supposed to be able to co-assemble in order to modulate their channel properties.[22] Thus, there can be a multitude of Kir2.x heteromultimers, and to date a wide range of single-channel conductances of inward rectifier channels have been reported in studies conducted on various mammalian myocytes, including human.[23–25] This variety at the individual channel level may contribute to the different stoichiometry of the tetrameric channels.[26] Because Kir2.1 is a major component of IK1 in the myocardium, we overexpressed the *KCNJ2* M301K mutant channels in NRVMs to examine the effects of the mutation on APD. Overexpression with WT alone resulted in shorter APD in comparison with non-transfected myocytes (*Figure 5B*). These results are consistent with a previously published report.[27] Notably, heterozygous overexpression with WT and M301K further

amplified the shortened APD (*Figure 5C*). These results were compatible with the electrophysiological changes assessed in HEK 293 cells, because the heterozygous WT/M301K channels showed a larger outward current than WT Kir2.1 channels under the physiological range of membrane potentials (*Figure 3*). Weak inward rectification observed in the heterozygous WT/M301K channels suggests that potassium ion can get through Kir2.1 channel at depolarized potential, probably resulting in loss of the action potential dome recorded in the *KCNJ2* WT/M301K-overexpressed group. The experiments were performed using a transient overexpression system that was different from the patient's heart, and the amount of overexpressed channels was difficult to be estimated accurately. But, these results are beneficial in understanding that the heterozygous *KCNJ2* M301K mutation could abbreviate APD and cause an extremely short-QT interval in the patient's ECG.

4.5 Clinical features of the index patient with *KCNJ2*-M301K

Regarding the clinical criteria for the diagnosis of SQTS, they have yet to be defined. However, we should consider SQTS in a patient presenting with a QTc <340 ms and other factors suggestive of arrhythmia (such as syncope or family history of sudden death).[28] A prominent clinical manifestation of SQTS is arrhythmias, such as AF

and VF.[1-5,7] In this patient, however, additional medical histories not limited to arrhythmias, such as severe mental retardation, abnormal proliferation of the oesophageal blood vessels, epilepsy, and Kawasaki' disease, were also documented. Because *KCNJ2* is known to be expressed in a variety of tissues, such as cardiac and skeletal muscle, the brain, arterial smooth muscle cells and developing bony structures of the craniofacial region, extremities, and vertebrae,[29-31] some of her compound disorders may be attributed to the *KCNJ2* mutation. In fact, loss-of-function mutations in *KCNJ2* cause Andersen—Tawil syndrome, which is characterized by prolonged repolarization, dysmorphic features, and periodic paralysis.[10,32] In the family of our female patient, we could not perform extensive genetic testing. We cannot exclude the possibility of the presence of other affected genes. Further analyses using knock-in mice or induced pluripotent stem cells would culminate monumental insight into the relationship between the *KCNJ2* M301K mutation and the patient's extra-cardiac phenotypes.

4.6 Conclusions

We described a novel *KCNJ2* gain-of-function mutation, M301K, in a patient with SQTS. Functional assays revealed no functional currents in the homozygous channels, whereas impaired inward rectification in the heterozygous channels manifested in larger outward currents, which is a novel mechanism predisposing SQTS.

Acknowledgements

References

1. Gussak I, Brugada P, Brugada J, Wright RS, Kopecky SL, Chaitman BR et al. Idiopathic short QT interval: a new clinical syndrome? *Cardiology* 2000;**94**:99–102.
2. Brugada R, Hong K, Dumaine R, Cordeiro J, Gaita F, Borggrefe M et al. Sudden death associated with short-QT syndrome linked to mutations in HERG. *Circulation* 2004; **109**:30–35.
3. Bellocq C, van Ginneken AC, Bezzina CR, Alders M, Escande D, Mannens MM et al. Mutation in the KCNQ1 gene leading to the short QT-interval syndrome. *Circulation* 2004;**109**:2394–2397.
4. Priori SG, Pandit SV, Rivolta I, Berenfeld O, Ronchetti E, Dhamoon A et al. A novel form of short QT syndrome (SQT3) is caused by a mutation in the KCNJ2 gene. *Circ Res* 2005;**96**:800–807.
5. Antzelevitch C, Pollevick GD, Cordeiro JM, Casis O, Sanguinetti MC, Aizawa Y et al. Loss-of-function mutations in the cardiac calcium channel underlie a new clinical entity characterized by ST-segment elevation, short QT intervals, and sudden cardiac death. *Circulation* 2007;**115**:442–449.
6. Templin C, Ghadri JR, Rougier JS, Baumer A, Kaplan V, Albesa M et al. Identification of a novel loss-of-function calcium channel gene mutation in short QT syndrome (SQTS6). *Eur Heart J* 2011;**32**:1077–1088.
7. Hong K, Piper DR, Diaz-Valdecantos A, Brugada J, Oliva A, Burashnikov E et al. De novo KCNQ1 mutation responsible for atrial fibrillation and short QT syndrome in utero. *Cardiovasc Res* 2005;**68**:433–440.
8. Garberoglio L, Giustetto C, Wolpert C, Gaita F. Is acquired short QT due to digitalis intoxication responsible for malignant ventricular arrhythmias? *J Electrocardiol* 2007; **40**:43–46.
9. Akao M, Ohler A, O'Rourke B, Marban E. Mitochondrial ATP-sensitive potassium channels inhibit apoptosis induced by oxidative stress in cardiac cells. *Circ Res* 2001; **88**:1267–1275.
10. Haruna Y, Kobori A, Makiyama T, Yoshida H, Akao M, Doi T et al. Genotype-phenotype correlations of KCNJ2 mutations in Japanese patients with Andersen-Tawil syndrome. *Hum Mutat* 2007;**28**:208.
11. Ma D, Tang XD, Rogers TB, Welling PA. An Andersen-Tawil syndrome mutation in Kir2.1 (V302M) alters the G-loop cytoplasmic K+ conduction pathway. *J Biol Chem* 2007;**282**:5781–5789.
12. Ballester LY, Benson DW, Wong B, Law IH, Mathews KD, Vanoye CG et al. Trafficking-competent and trafficking-defective KCNJ2 mutations in Andersen syndrome. *Hum Mutat* 2006;**27**:388.
13. Pegan S, Arrabit C, Zhou W, Kwiatkowski W, Collins A, Slesinger PA et al. Cytoplasmic domain structures of Kir2.1 and Kir3.1 show sites for modulating gating and rectification. *Nat Neurosci* 2005;**8**:279–287.
14. Tai K, Stansfeld PJ, Sansom MS. Ion-blocking sites of the Kir2.1 channel revealed by multiscale modeling. *Biochemistry* 2009;**48**:8758–8763.
15. Fujiwara Y, Kubo Y. Functional roles of charged amino acid residues on the wall of the cytoplasmic pore of Kir2.1. *J Gen Physiol* 2006;**127**:401–419.
16. Gollob MH, Redpath CJ, Roberts JD. The short QT syndrome: proposed diagnostic criteria. *J Am Coll Cardiol* 2011;**57**:802–812.
17. Xia M, Jin Q, Bendahhou S, He Y, Larroque MM, Chen Y et al. A Kir2.1 gain-of-function mutation underlies familial atrial fibrillation. *Biochem Biophys Res Commun* 2005;**332**:1012–1019.
18. Matsuda H, Saigusa A, Irisawa H. Ohmic conductance through the inwardly rectifying K channel and blocking by internal Mg2+. *Nature* 1987;**325**:156–159.
19. Horie M, Irisawa H, Noma A. Voltage-dependent magnesium block of adenosine-triphosphate-sensitive potassium channel in guinea-pig ventricular cells. *J Physiol* 1987;**387**:251–272.
20. Hille B. *Ion Channels of Excitable Membranes*. Sunderland: Sinauer Associates, 2001.
21. Robertson JL, Palmer LG, Roux B. Long-pore electrostatics in inward-rectifier potassium channels. *J Gen Physiol* 2008;**132**:613–632.
22. Liu Y, Fowler CD, Wang Z. Ontogeny of brain-derived neurotrophic factor gene expression in the forebrain of prairie and montane voles. *Brain Res Dev Brain Res* 2001; **127**:51–61.
23. Nakamura TY, Artman M, Rudy B, Coetzee WA. Inhibition of rat ventricular IK1 with antisense oligonucleotides targeted to Kir2.1 mRNA. *Am J Physiol* 1998;**274**: H892–H900.
24. Picones A, Keung E, Timpe LC. Unitary conductance variation in Kir2.1 and in cardiac inward rectifier potassium channels. *Biophys J* 2001;**81**:2035–2049.
25. Wible BA, De Biasi M, Majumder K, Taglialatela M, Brown AM. Cloning and functional expression of an inwardly rectifying K+ channel from human atrium. *Circ Res* 1995;**76**: 343–350.
26. Preisig-Muller R, Schlichthorl G, Goerge T, Heinen S, Bruggemann A, Rajan S et al. Heteromerization of Kir2.x potassium channels contributes to the phenotype of Andersen's syndrome. *Proc Natl Acad Sci USA* 2002;**99**:7774–7779.
27. Miake J, Marban E, Nuss HB. Functional role of inward rectifier current in heart probed by Kir2.1 overexpression and dominant-negative suppression. *J Clin Invest* 2003;**111**:1529–1536.
28. Viswanathan MN, Page RL. Short QT: when does it matter? *Circulation* 2007;**116**: 686–688.
29. Raab-Graham KF, Radeke CM, Vandenberg CA. Molecular cloning and expression of a human heart inward rectifier potassium channel. *Neuroreport* 1994;**5**:2501–2505.
30. Karkanis T, Li S, Pickering JG, Sims SM. Plasticity of KIR channels in human smooth muscle cells from internal thoracic artery. *Am J Physiol Heart Circ Physiol* 2003;**284**: H2325–H2334.
31. Karschin C, Karschin A. Ontogeny of gene expression of Kir channel subunits in the rat. *Mol Cell Neurosci* 1997;**10**:131–148.
32. Plaster NM, Tawil R, Tristani-Firouzi M, Canun S, Bendahhou S, Tsunoda A et al. Mutations in Kir2.1 cause the developmental and episodic electrical phenotypes of Andersen's syndrome. *Cell* 2001;**105**:511–519.

SIGNALING AND CELL PHYSIOLOGY

Regulatory mechanisms underlying the modulation of GIRK1/GIRK4 heteromeric channels by P2Y receptors

Jie Wu · Wei-Guang Ding · Hiroshi Matsuura · Minoru Horie

Abstract The muscarinic K^+ channel ($I_{K,ACh}$) is a hetero-tetramer composed of GIRK1 (Kir3.1) and GIRK4 (Kir3.4) subunits of a G protein-coupled inwardly rectifying channel, and plays an important role in mediating electrical responses to the vagal stimulation in the heart. $I_{K,ACh}$ displays biphasic changes (activation followed by inhibition) through the stimulation of the purinergic P2Y receptors, but the regulatory mechanism involved in these modulation of $I_{K,ACh}$ by P2Y receptors remains to be fully elucidated. Various P2Y receptor subtypes and GIRK1/GIRK4 (I_{GIRK}) were co-expressed in Chinese hamster ovary cells, and the effect of stimulation of P2Y receptor subtypes on I_{GIRK} were examined using the whole-cell patch-clamp method. Extracellular application of 10 μM ATP induced a transient activation of I_{GIRK} through the $P2Y_1$ receptor, which was completely abolished by pretreatment with pertussis toxin. ATP initially caused an additive transient increase in ACh-activated I_{GIRK} (via M_2 receptor), which was followed by subsequent inhibition. This inhibition of I_{GIRK} by ATP was attenuated by co-expression of regulator of G-protein signaling 2, or phosphatidylinositol-4-phosphate-5-kinase, or intracellular phosphatidylinositol 4,5-bisphosphate loading, but not by the exposure to protein kinase C inhibitors. $P2Y_4$ stimulation also persistently suppressed the ACh-activated I_{GIRK}. In addition, I_{GIRK} evoked by the stimulation of the $P2Y_4$ receptor exhibited a transient activation, but that evoked by the stimulation of $P2Y_2$ or $P2Y_{12}$ receptor showed a rather persistent activation. These results reveal (1) that $P2Y_1$ and $P2Y_4$ are primarily coupled to the G_q-phospholipase C-pathway, while being weakly linked to $G_{i/o}$, and (2) that $P2Y_2$ and $P2Y_{12}$ involve $G_{i/o}$ activation.

Jie Wu and Wei-Guang Ding have contributed equally to this work.

J. Wu
Department of Pharmacology,
Medical School of Xi'an Jiaotong University,
Xi'an, Shaanxi 710061, People's Republic of China

J. Wu · W.-G. Ding · H. Matsuura (✉)
Department of Physiology, Shiga University of Medical Science,
Otsu, Shiga 520-2192, Japan
e-mail: matuurah@belle.shiga-med.ac.jp

J. Wu · M. Horie (✉)
Department of Cardiovascular and Respiratory Medicine,
Shiga University of Medical Science,
Otsu, Shiga 520-2192, Japan
e-mail: horie@belle.shiga-med.ac.jp

Abbreviations

ACh	Acetylcholine
$I_{K,ACh}$	Muscarinic K^+ channel
PLC	Phospholipase C
PKC	Protein kinase C
PIP$_2$	Phosphatidylinositol 4,5-bisphosphate
PTX	Pertussis toxin
PI4P-5K	Phosphatidylinositol-4-phosphate-5-kinase
CHO	Chinese hamster ovary
AC	Adenylyl cyclase
WT	Wild type
GFP	Green fluorescent protein
ATP	Adenosine triphosphate
UTP	Uridine triphosphate
RGS$_2$	Regulator of G-protein signaling 2
GIRK	G protein-activated inward rectifier K^+ channel

🙋 Springer

Introduction

The muscarinic K^+ channel ($I_{K,ACh}$) is a heterotetramer that comprises Kir3.1 and Kir3.4 subunits (encoded by GIRK1 and GIRK4, respectively) of G protein-coupled inwardly rectifying channel. $I_{K,ACh}$ plays an important role in mediating negative inotropic, chronotropic, and dromotropic responses to the vagal neurotransmitter acetylcholine (ACh) in the heart [20]. Previous reports indicate that adenosine 5'-triphosphate (ATP) produces dual effects on $I_{K,ACh}$: a transient activation followed by a persistent inhibition, in guinea pig atrial cells [13, 24, 44]. Like other neurotransmitters such as ACh [34, 35] and adenosine [21, 24], ATP activates the membrane receptors coupled to the $I_{K,ACh}$ channel proteins through a pertussis toxin (PTX) sensitive heterotetrameric G protein, thus leading to the dissociation of the heterotrimeric G-protein complex into its α and $\beta\gamma$ subunits that can interact with the channel and cause an increase in open-state probability of the channel [5, 24, 42]. Conversely, $I_{K,ACh}$ is persistently inhibited by ATP following the transient activation. Previous studies using guinea pig atrial cells [25, 44] demonstrated that the inhibition of $I_{K,ACh}$ by ATP is associated with activation of the P2Y receptors that are coupled to a PTX-insensitive G protein leading to activation of G_q-phospholipase C (PLC) signaling pathway. However, the modulatory mechanism underlying the inhibition of $I_{K,ACh}$ by P2Y receptor subtype stimulation has yet to be fully elucidated.

P2Y receptors belong to G protein-coupled P2 purinergic receptors that can be activated by purine or pyrimidine nucleotides. Eight P2Y receptor subtypes (P2Y$_{1, 2, 4, 6, 11, 12, 13}$ and $_{14}$) have been cloned from mammalian cells, and all of them are expressed in heart tissues and associated with the extracellular signaling pathway [3, 10, 30, 37]. Several studies have so far indicated that ATP elicits diverse functional responses in various types of tissues including cardiac cells [10, 26, 27]. However, the functional coupling correlates of the involved P2Y receptor subtypes in cardiac cells is still a topic of debate and remains difficult in native cell due to the restricted availability of subtype-selective ligands and/or blockers.

The present study was undertaken to further explore the inhibitory mechanism of $I_{K,ACh}$ using Chinese hamster ovary (CHO) cells heterologously co-expressed with GIRK1/GIRK4 and different P2Y receptor subtypes. The result reveals that stimulation of P2Y$_1$ or P2Y$_4$ receptor subtype markedly inhibited ACh-activated I_{GIRK} currents by G_q-PLC pathway signaling, although the two receptors were also weakly coupled to $G_{i/o}$ protein to transiently activate I_{GIRK}. On the contrary, P2Y$_2$ and P2Y$_{12}$ receptor subtypes were coupled with $G_{i/o}$ protein to persistently activate I_{GIRK}.

Materials and methods

Heterologous expression of cDNA in CHO cells

Full-length cDNA encoding rat GIRK1 subcloned into the pCI expression vector was a kind gift from Dr. LY Jan (Department of Physiology and Biochemistry, Howard Hughes Medical Institute, University of California). Full-length cDNA encoding rat GIRK4 subcloned into the pCDNA3 expression vector was kindly provided by Dr. JP Adelman (Department of Molecular and Medical Genetics, Oregon Health and Sciences University). Full-length cDNA encoding rat type I phosphatidylinositol-4-phosphate-5-kinase (PI4P-5K) subcloned into pCDNA3 expression vector was generously donated by Dr. Y Oka (Third Department of Internal Medicine, Yamaguchi University School of Medicine, Japan). Full-length cDNA encoding human M_2, α_1, P2Y$_1$, P2Y$_2$, P2Y$_4$, P2Y$_{12}$ receptors and regulator of G protein signaling 2 (RGS$_2$) subcloned individually into pCDNA3.1$^+$ were all obtained from the University of Missouri–Rolla cDNA Resource Center (Rolla, MO). The experimental cDNAs were transiently transfected into CHO cells together with green fluorescent protein (GFP) cDNA [0.5 µg GFP +1 µg GIRK1+1 µg GIRK4+1 µg P2Ys (or α_1)+1 µg M_2] by using Lipofectamine (Invitrogen Life Technologies, Inc. Carlsbad, CA, USA) according to the manufacturer's instructions. Two micrograms of PI4P-5K or RGS$_2$ cDNA was co-transfected in subset experiments. The transfected cells were cultured in DMEM/Ham's F-12 medium (Nakalai Tesque Inc., Kyoto, Japan) supplemented with 10% fetal bovine serum (GIBCO) and antibiotics (100 U/ml penicillin and 100 µg/ml streptomycin) in a humidified incubator with 5% CO_2 and 95% air at 37°C. The cultures were passaged every 4 to 5 days using a brief trypsin–EDTA treatment. The trypsin-EDTA treated cells were seeded onto glass coverslips in a petri dish for later patch-clamp experiments.

Solutions and chemicals

The pipette solution contained (mM) 70 potassium aspartate, 40 KCl, 10 KH_2PO_4, 1 $MgSO_4$, 3 Na_2-ATP (Sigma), 0.1 Li_2-GTP (Roche Diagnostics GmbH, Mannheim, Germany), 5 EGTA, and 5 Hepes, and pH was adjusted to 7.2 with KOH. The extracellular solution contained (mM) 140 NaCl, 5.4 KCl, 1.8 $CaCl_2$, 0.5 $MgCl_2$, 0.33 NaH_2PO_4, 5.5 glucose, and 5.0 Hepes, and pH was adjusted to 7.4 with NaOH. Agents added to the extracellular solutions included ACh (Sigma Chemical Co., St. Louis, MO, USA), ATP (Sigma), uridine triphosphate (UTP, Sigma), bisindolylmaleimide 1 (BIS-1, Sigma), chelerychrine (CHE, Sigma), and phenylephrine (PHE, Sigma). ACh, ATP, UTP, and PHE were dissolved in the distilled water to yield 10 mM or 30

mM stock solutions. BIS-1 and CHE were dissolved in dimethyl sulfoxide (DMSO, Sigma) to yield stock solutions of 200 μM and 5 mM, respectively. Phosphatidylinositol 4,5-bisphosphate (PIP$_2$; Calbiochem, San Diego, CA, USA) was directly dissolved in the control pipette solution at a concentration of 50 μM with 30 min sonication on ice. In a subset of experiments, the cells were pre-incubated with 5 μg/ml PTX (Seikagaku, Japan) for at least 2 h to inhibit a PTX-sensitive G protein, as previously described [16].

Electrophysiological recordings and data analysis

The cells attached to glass coverslips were transferred to a 0.5-ml recording chamber perfused with extracellular solution at 1–2 ml/min after 48 h of transfection. The chamber was mounted on the stage of an inverted microscope (ECLIPSE TE2000-U; Nikon, Tokyo, Japan) and maintained at 25°C. Patch-clamp experiments were conducted on GFP-positive cells. Whole-cell membrane currents were recorded with an EPC-8 patch-clamp amplifier (HEKA, Lambrecht, Germany), and data were low-pass filtered at 1 kHz, acquired at 5 kHz through an LIH-1600 analog-to-digital converter (HEKA) and stored on a hard disc drive, using the PulseFit software program (HEKA). Patch pipettes were fabricated from borosilicate glass capillaries (Narishige, Japan) using a horizontal microelectrode puller (P-97; Sutter Instrument Co., USA), and the tips were then fire-polished using a microforge. Patch pipettes had a resistance of 2.5–4.0 MΩ when filled with the pipette solution. Membrane currents were measured at a holding potential of −40 mV or during the voltage ramp protocol (dV/dt=±0.4 V/s), which consisted of an ascending (depolarizing) phase from the holding potential to +50 mV followed by a descending (hyperpolarizing) phase to −130 mV. The current–voltage (I–V) relationship was determined during descending phase.

All of the averaged data are expressed as the mean ± SEM, with the number of experiments shown in parentheses. Statistical comparisons were analyzed using either Student's unpaired t test or ANOVA followed by Dunnett's *post hoc*, as appropriate. Differences were considered to be statistically significant if a value of $P<0.05$ was obtained.

Results

The nature of I_{GIRK} during exposure to ATP in CHO cells expressing P2Y$_1$ receptor

The effect of extracellular ATP on I_{GIRK} was examined in cells transfected with P2Y$_1$ receptor by measuring whole-cell membrane currents at a holding potential of −40 mV and during hyperpolarizing voltage ramps from +50 to

−130 mV. The bath application of 10 μM ATP initially evoked a rapid outward shift of the holding current (I_{GIRK} activation), which then progressively declined to the baseline level within ~1–2 min (a subsequent inward shift, Fig. 1a) despite the continued presence of the agonist.

Figure 1b illustrates the membrane currents during hyperpolarizing voltage ramps, recorded before and during application of ATP. The membrane current was calculated by digital subtraction of the current traces under control conditions from that shortly after ATP application and showed an inward rectification (Fig. 1c). $I_{K,ACh}$ is activated by a membrane-delimited pathway involving a PTX-sensitive G protein (G$_{i/o}$) in guinea-pig atrial myocytes [24]. The present experiment also found that pre-exposure to 5 μg/ml PTX for 2 h abolished the action of extracellular ATP (Fig. 1d), suggesting that a PTX-sensitive G protein mediates the activation of I_{GIRK} by P2Y$_1$ receptor stimulation.

The functional regulation of P2Y$_1$ receptor was further analyzed using 10 μM ACh to induce an activation of I_{GIRK} at −40 mV (Fig. 2a). The further addition of ATP initially had an additive effect on ACh-activated I_{GIRK} but then markedly inhibited the current (Fig. 2a; the number of cells
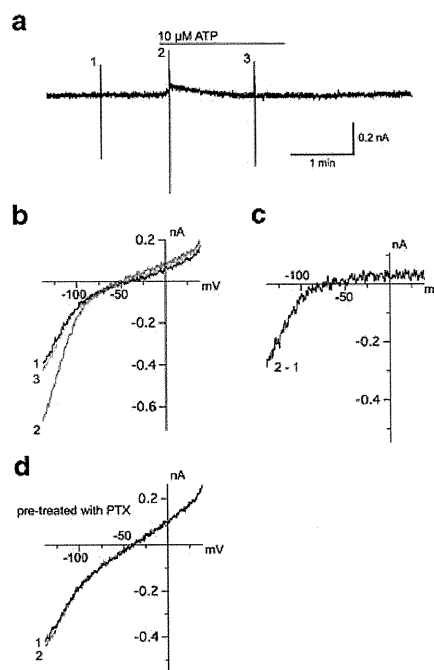

Fig. 1 Effect of ATP on the activation of I_{GIRK} in CHO cells transfected with P2Y$_1$ receptor. **a** The whole-cell currents recorded at a holding potential of −40 mV and during exposure to 10 μM ATP. **b** Superimposed I–V relationships measured during the voltage ramps applied at the points indicated by numbers (*1–3*) in panel (**a**). **c** I–V relationship obtained by digital subtraction of current traces as indicated. **d** After pretreatment with 5 μg/ml PTX for 2 h, the I–V relationships were measured during the voltage ramps
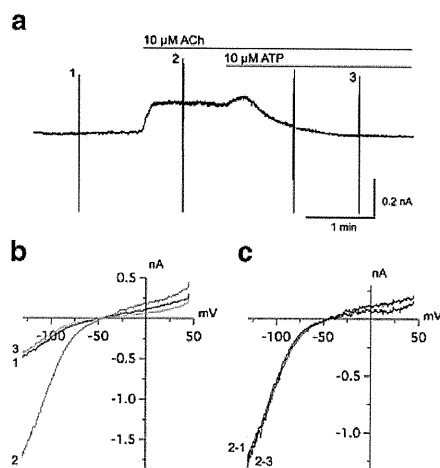
Fig. 2 Inhibition of ACh-activated I_{GIRK} by ATP. **a** The whole-cell currents recorded at a holding potential of −40 mV and during voltage ramps applied before (*1*), during exposure to 10 µM ACh (*2*), and after further addition of 10 µM ATP (*3*). **b** Superimposed *I–V* relationships measured during the voltage ramps applied at the points indicated by numerals (*1–3*) in panel (**a**). **c** Superimposed *I–V* relationships for the difference currents obtained by digital subtraction of current records as indicated. The voltage ramp traces were truncated for the purpose of presentation

positively responded to ATP was 18/19). The ACh-activated maximal I_{GIRK} was decreased by 92.44±10.61% (*n*=19), when measured 3 min after application of 10 µM ATP, which indicates that external ATP almost inhibited the ACh-activated I_{GIRK}. Figure 2b and c show that the ACh-activated I_{GIRK} current also exhibited an inwardly rectifying *I–V* relationship, which is consistent with the properties of $I_{K,ACh}$ in guinea-pig atrial myocytes. In addition, I_{GIRK} isolated by digital subtraction of the currents in the presence of ACh from that after ATP application also exhibited an inwardly rectifying *I–V* relationship.

In different sets of experiments, we examined the background currents and the expression ability of our CHO cell expression system. The results show that bath application of ACh and ATP could not induce any discernible currents in non-transfected cells (Fig. S1a) and in cells transfected only with GFP + GIRK1/GIRK4 (Fig. S1b). However, ACh evoked persistent I_{GIRK} currents in cells transfected with GFP + GIRK1/GIRK4 + M₂ (Fig. S1c), which was consistently inhibited by ATP when co-transfected with P2Y₁ in addition to GIRK subunits and M₂ (Fig. S1d). Figure S1e shows the representative image of the cells showing GFP expression. On the other hand, the inhibition of I_{GIRK} currents was not observed in cells without P2Y₁ transfection (Fig. S1c). These results indicate that functional expression of intrinsic P2Y and M₂ receptors was almost null in our CHO cell expression system, and all plasmids were successfully expressed in our cells. To exclude the possibility that

the activation of I_{GIRK} was affected by G protein-coupled receptor–G protein interaction, we observed the effects of ATP on ACh-activated I_{GIRK} in CHO cells co-transfected lower doses (0.2–0.5 µg) of P2Y₁ together with 0.5 µg GFP +1 µg GIRK1/GIRK4+1 µg M₂. Figure S1f shows that the inhibition of ACh-activated I_{GIRK} by ATP in cells co-transfected with 0.2 µg P2Y₁ is almost the same as that co-transfected with 1 µg P2Y₁.

The modulation of RGS₂ on ATP-induced inhibition of I_{GIRK}

Regulators of G-protein signaling (RGS) proteins modulate the signal transduction via G protein-coupled receptors (GPCR). These proteins enhance GTP hydrolysis by accelerating the intrinsic GTPase activity of Gα-subunit, and thereby terminate the G protein activation cycle [4, 31, 39]. RGS₂ (one of the important inhibitor of $G_q\alpha$ subunit) was co-transfected with GIRK1/GIRK4, M₂ and P2Y₁ cDNAs to explore the inhibitory mechanism of ATP on I_{GIRK}. Figure 3a shows that the inhibitory action of ATP on ACh-activated I_{GIRK} was significantly attenuated with the co-expression of RGS₂. Figure 3c shows that the inhibitory degree of the ACh-activated I_{GIRK} was only 50.7± 9.1% (*n*=15) 3 min after exposure to 10 µM ATP, which
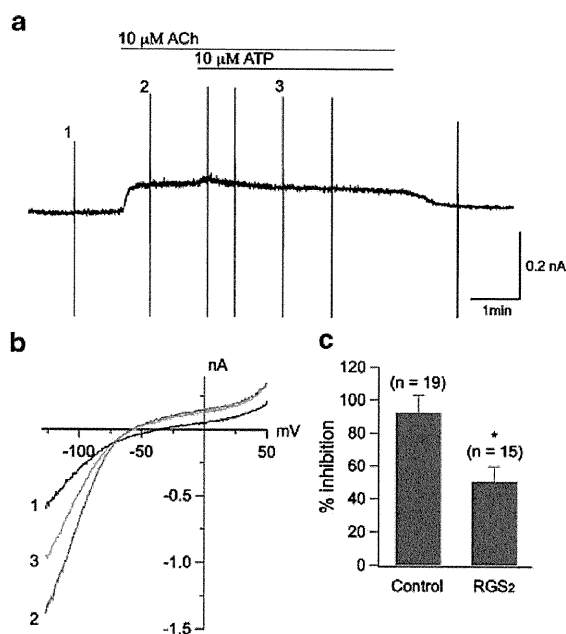

Fig. 3 The modulation of RGS₂ on the ATP-induced inhibition of I_{GIRK}. **a** Whole-cell currents recorded in CHO cell co-transfected with RGS₂ at a holding potential of −40 mV. **b** Superimposed *I–V* relationships measured during the voltage ramps applied at the points indicated by numerals (*1–3*) in panel (**a**). **c** ATP-induced inhibition of I_{GIRK} (*$^*P<0.05$ vs. control)

is significantly ($P<0.05$) lower than that of control ($92.44\pm10.61\%$, $n=19$). Therefore, the activation of G_q protein is involved in the ATP-induced inhibition of I_{GIRK}. Besides, our supplementary experiment data observed in CHO cells co-transfected 1 μg M_1 receptor (coupled with G_q) together with 0.5 μg GFP+1 μg GIRK1+1 μg GIRK4+1 μg M_2 (Fig. S3a) also supports the result that the activation of G_q protein is involved in the agonist-induced inhibition of I_{GIRK} in this experiment.

In order to further confirm the result that co-expression of RGS_2 led to the inhibition of the signal transduction via G_q protein-coupled receptors in our cell expression system, we co-transfected GFP + GIRK1/GIRK4+M_2+RGS_2 together with α_1-adrenergic receptor that has been generally accepted to be coupled to G_q [8]. Similar to the inhibition of ACh-activated I_{GIRK} currents by ATP, bath application of PHE (a selective α_1 receptor agonist, 30 μM) significantly inhibited the ACh-activated I_{GIRK} currents by $94.8\pm10.1\%$ ($n=7$) in cells co-expressing α_1 receptor (Fig. S2a), whereas only by $40.3\pm5.4\%$ ($n=5$, $P<0.01$) in cells co-expressing RGS_2+α_1 receptor (Fig. S2b), implicating that the attenuation of I_{GIRK} inhibition by ATP in cells co-expressing RGS_2 is involved in blockade of G_q protein in our experiment.

Role of membrane PIP_2 in ATP-induced decline of I_{GIRK}

A previous study indicated that ATP receptor stimulation could inhibit the $I_{K,ACh}$ channels through depletion of membrane PIP_2 in guinea pig atrium [44]. PI4P-5K (the enzyme that catalyzes PIP_2 synthesis [11]) was co-expressed with GIRK1/GIRK4, M_2, and $P2Y_1$ cDNAs. Figure 4a shows that the co-expression of PI4P-5K markedly ($P<0.01$) prevented the inhibitory action of ATP on ACh-activated I_{GIRK}, compared with that in control ($55.2\pm10.0\%$, $n=13$ vs. $92.44\pm10.61\%$, $n=19$; Fig. 4c). This result is consistent with the view that a characteristic progressive decline of I_{GIRK} in the presence of extracellular ATP is mediated through the depletion of membrane PIP_2.

If the reduction in membrane PIP_2 underlies the decline of I_{GIRK} during exposure to ATP, intracellular loading of exogenous PIP_2 may attenuate the inhibitory action of ATP on ACh-activated I_{GIRK}. As demonstrated in Fig. 5a and b, intracellular dialysis of 50 μM PIP_2 for 5–7 min through a recording pipette significantly reduced the inhibition degree of ACh-activated I_{GIRK} by ATP. The inhibition of I_{GIRK} (Fig. 5c) only reached $18.2\pm6.4\%$ ($n=5$) 3 min after bath application of 10 μM ATP, which is markedly ($P<0.01$) lower than that of the control ($92.44\pm10.61\%$, $n=19$). This result further indicates that the reduction in membrane PIP_2 is closely linked to the inhibitory action of ATP on I_{GIRK}.

PKC activation was previously reported to produce inhibitory action on $I_{K,ACh}$ [14, 22, 31, 35]. In our experiments, however, bath application of two different PKC
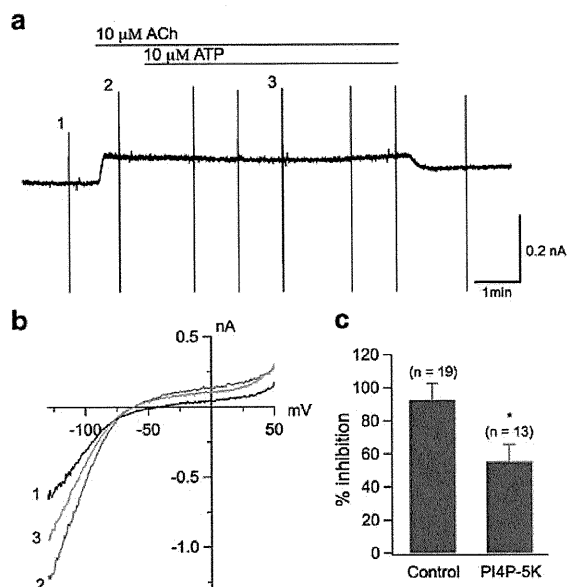

Fig. 4 Co-expression of PI4P-5K attenuated the ATP-induced inhibition of I_{GIRK}. a The whole-cell currents recorded in CHO cell co-transfected with PI4P-5K in the presence of ACh and ATP at a holding potential of −40 mV. b Superimposed I–V relationships measured during the voltage ramps applied at the points indicated by numerals (1–3) in panel (a). c ATP-induced inhibition of I_{GIRK} (*$P<0.05$ vs. control)
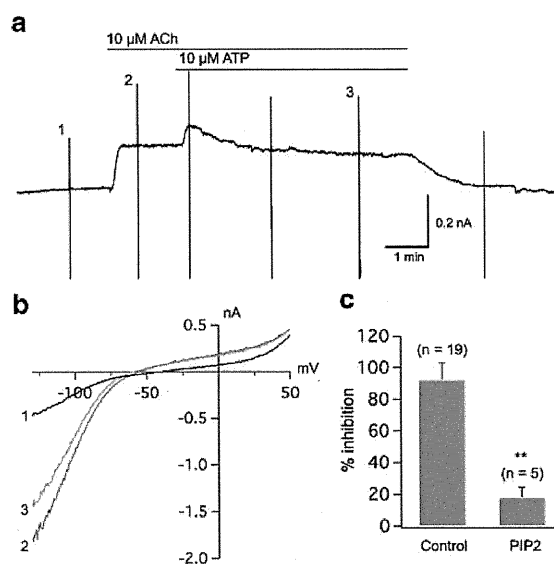

Fig. 5 Effect of PIP_2 (intracellularly loaded) on the ATP-induced inhibition of I_{GIRK}. a Whole-cell currents recorded with PIP_2 intracellular dialysis for 5–7 min at a holding potential of −40 mV, and then in the presence of ACh and ATP. b Superimposed I–V relationships measured during the voltage ramps applied at the points indicated by numerals (1–3) in panel (a). c ATP-induced inhibition of I_{GIRK} (**$P<0.01$ vs. control)

inhibitors, bisindolylmaleimide (BIS-1, 200 nM, Fig. 6a and b) and chelerythrine (CHE, 5 μM, Fig. 6b), did not significantly alter the inhibition degree of ACh-activated I_{GIRK} by ATP (control, 92.44±10.61%, n=19; BIS-I, 95.7±15.0%, n=7; CHE, 92.3±17.5%, n=6), thus suggesting that PKC activation is not involved in the ATP-induced inhibition of I_{GIRK} [7, 28].

Effects of P2Y receptor subtype stimulation on I_{GIRK}

Different P2Y receptor subtpes, namely P2Y$_2$, P2Y$_4$, and P2Y$_{12}$, were respectively transfected together with GIRK1/ GIRK4 channels to explore the effects of the P2Y receptor stimulation on I_{GIRK}. In the experiment, 10 μM UTP was used as an alternative to ATP to activate P2Y$_2$ and P2Y$_4$ receptors because it seems that these two receptors are more sensitive to UTP [38, 41]. Figure 7a shows the representative I_{GIRK} traces elicited by stimulating P2Y$_2$, P2Y$_4$, and P2Y$_{12}$ receptors, respectively. The persistent I_{GIRK} currents elicited by the stimulation of P2Y$_2$ or P2Y$_{12}$ receptor suggest that little membrane PIP$_2$ was depleted, whereas the current evoked by the stimulation of P2Y$_4$ receptor was transient, which suggests that depletion of membrane PIP$_2$ occurred. Figure 7b and c shows the amplitudes of I_{GIRK} normalized to the peak amplitude one minute (I_{1min}/I_{peak}) and 3 min (I_{3min}/I_{peak}) after application of an agonist. The normalized amplitude of I_{GIRK} for P2Y$_2$ or P2Y$_{12}$ was significantly (P<0.01) larger than that of P2Y$_1$ both 1 and 3 min after application of an agonist, whereas the amplitude of I_{GIRK} for P2Y$_1$ or P2Y$_4$ 3 min after receptor stimulation was significantly (P<0.05) lower than that for the same receptor 1 min after receptor stimulation.
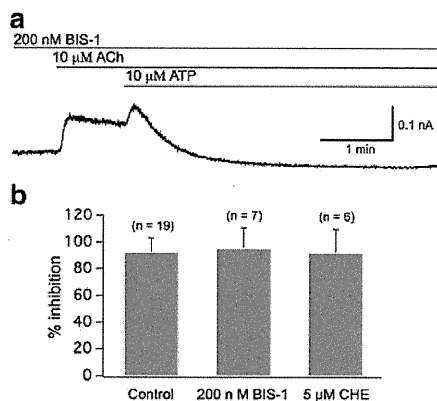

Fig. 6 PKC inhibitors did not attenuate the ATP-induced inhibition of I_{GIRK}. **a** The whole-cell currents recorded in CHO cell pre-treated with 200 nM BIS-1 in the presence of ACh and ATP at a holding potential of −40 mV. **b** ATP-induced inhibition of I_{GIRK} in the presence of 200 nM BIS-1 or 5 μM CHE
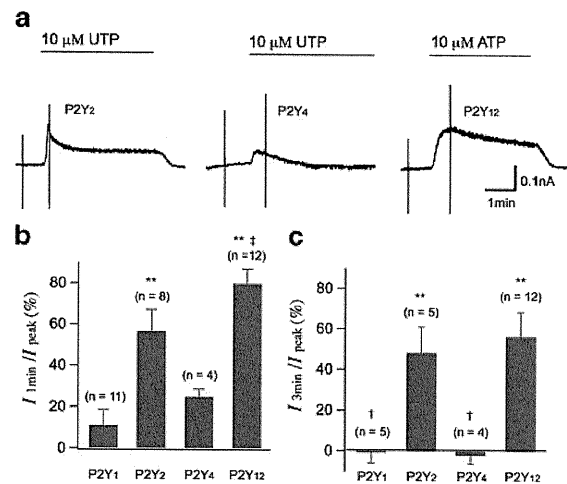

Fig. 7 Comparison of I_{GIRK} currents evoked by stimulating different P2Y receptor subtypes. **a** The whole-cell currents in CHO cells transfected with P2Y$_2$, P2Y$_4$, and P2Y$_{12}$ receptor subtypes at a holding potential of −40 mV. **b** Inhibition of I_{GIRK} 1 min after stimulation of P2Y$_2$, P2Y$_4$, and P2Y$_{12}$ receptors. **c** Inhibition of I_{GIRK} 3 min after stimulation of P2Y$_2$, P2Y$_4$, and P2Y$_{12}$ receptors (**P<0.01 vs. P2Y$_1$ or P2Y$_4$; $^{\ddagger}P$<0.05 vs. P2Y$_2$; $^{\dagger}P$<0.05 vs. I_{1min}/I_{peak})

Treatment with 10 μM ACh was first used to induce an I_{GIRK} current at −40 mV, and then 10 μM UTP or ATP was employed to stimulate P2Y$_2$, P2Y$_4$, or P2Y$_{12}$ to further examine the effects of P2Y$_s$ receptor stimulation on ACh-activated I_{GIRK}. Figure 8a and b shows that the nature of the current evoked by stimulating P2Y$_4$ receptor with UTP was almost the same as that elicited by stimulating P2Y$_1$ (Fig. 2). The inhibitory degree of ACh-activated I_{GIRK} by the stimulation of P2Y$_4$ was 99.6±22.5% (n=5), which was similar to that evoked by the stimulation of P2Y$_1$ receptor (Fig. 8c). Figure S3b and c shows that addition of an agonist (ATP or UTP) caused the ACh-activated I_{GIRK} to increase further (there was 1/13 cell co-transfected with P2Y$_2$ that did not respond to UTP). The addition activation of I_{GIRK} by the stimulation of P2Y$_2$ declined slightly, but still much higher than the ACh-activated I_{GIRK} level 3 min after treatment with UTP (Fig. S3b). On the other hand, the addition activation of I_{GIRK} by the stimulation of P2Y$_{12}$ almost did not decline (Fig. S3c).

Discussion

The activation of $I_{K,ACh}$ is due to the activation of G$_{i/o}$ protein [34]. The rapid activation phase of $I_{K,ACh}$ evoked by exposure to ATP is caused by stimulation of P2Y receptor, leading to a membrane-delimited, G$_{i/o}$-mediated channel activation in guinea-pig atrial myocytes [14, 25, 44]. However, there is no consensus on the mechanism of $I_{K,ACh}$
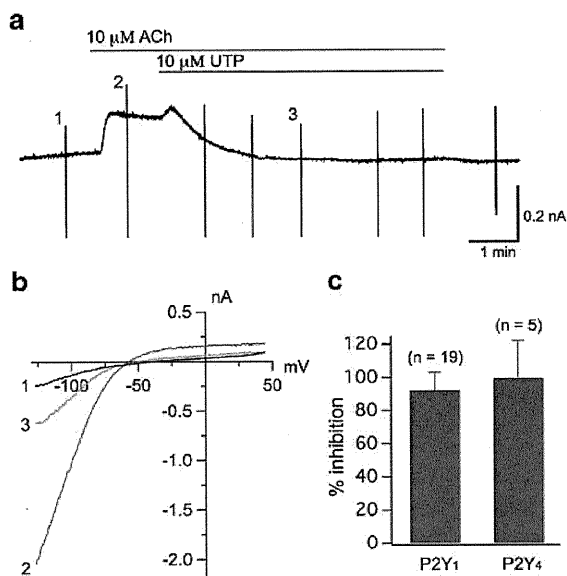
a

b

c

Fig. 8 Effect of P2Y$_4$ stimulation on ACh-activated I_{GIRK}. **a** The whole-cell currents recorded at a holding potential of −40 mV, and in the presence of ACh and UTP. **b** Superimposed I–V relationships measured during the voltage ramps applied at the points indicated by numerals (*1–3*) in panel (**a**). **c** Inhibitory degree of I_{GIRK} by the stimulation of P2Y$_1$ and P2Y$_4$ receptors

inhibition produced by agonists. Several groups [7, 14, 18, 25, 29, 44] reported that activation of PLC contributes to the inhibition of $I_{K,ACh}$ by decreasing membrane PIP$_2$. However, others [15, 23, 32, 36] suggest that the downstream activation of PKC underlies the inhibition of $I_{K,ACh}$. There are also some pieces of evidence to suggest that reduction in membrane PIP$_2$ and PKC activation are both involved in the $I_{K,ACh}$ inhibition by agonists such as carbachol [22] and ACh [17].

A previous study in the guinea-pig atrium indicated that the inhibition of $I_{K,ACh}$ by extracellular ATP is attenuated by blocking PLC activity with compound 48/80 and by exogenously adding PIP$_2$ in the atrial myocytes [44]. This observation suggests that the ATP-induced activation of PLC and the concomitant reduction of PIP$_2$ contribute to the inhibition of $I_{K,ACh}$ by ATP. In addition, RGS$_2$ protein is one of the important inhibitor of the G$_q\alpha$ subunit and terminates G$_q$ signaling through its GTPase-activating protein mechanism [4, 31, 39]. The present experiment found that co-expression of RGS$_2$ significantly reduced the ATP-induced inhibition of I_{GIRK}, thus confirming the view that the inhibition of I_{GIRK} by ATP is mediated through the G$_q$ protein-coupled P2Y receptors in native cardiac myocytes [14, 25]. The present study also demonstrated that the ATP-induced inhibition of I_{GIRK} is markedly attenuated by both co-expression of PI4P-5K and intracellular dialysis with PIP$_2$ in CHO

cells. These data are consistent with a previous study in guinea-pig atrial myocytes [44] and support the view that a decrease in membrane PIP$_2$ is closely linked to the ATP-induced inhibition of $I_{K,ACh}$. In contrast to the study of Keselman et al. [17], however, the PKC inhibitor BIS-1 and CHE did not alter the inhibition of ATP on ACh-activated I_{GIRK}, thus indicating PKC activation might not be involved in the inhibition of I_{GIRK} by ATP [9, 28]. Taken together, the current data fully support the hypothesis that the reduction in membrane PIP$_2$ via activation of G$_q$-PLC is mainly responsible for the inhibition of $I_{K,ACh}$ channels by externally applying ATP.

Previous reports have indicated that P2Y$_1$, P2Y$_2$, and P2Y$_4$ receptor subtypes are coupled to PTX-insensitive G$_q$ proteins that activate PLC and then produce a fall in membrane PIP$_2$ levels, whereas P2Y$_{12}$ receptor is only coupled to PTX-sensitive G$_{i/o}$ protein to inhibition of adenylate cyclase [1, 9, 37, 41]. However, the coupling to signaling transduction pathways appears to be much more complex. An example is that the G$_q$-coupled P2Y$_1$ receptor, known to inhibit GIRK channels, efficiently activates GIRK1/GIRK2 channels in cultured rat sympathetic neurons [12]. A sequence analysis also indicates that the two regions (the third intracellular loop and the C-terminal tail), implicated in G protein specificity, vary greatly among the P2Y receptor subtypes [40]. The present study found that the stimulation of P2Y$_1$ or P2Y$_4$ receptor evoked a transient activation of I_{GIRK} followed by a persistent inhibition (Figs. 1a and 7a), thus suggesting that a large amount of membrane PIP$_2$ was consumed via activation of G$_q$-PLC pathway. This result might implicate that the two receptors are mainly coupled to G$_q$ protein. Contrary to previous reports [1, 9, 37, 41], however, the activation phase of I_{GIRK} evoked by the stimulation of these two receptors reflects the existence of G$_{i/o}$ coupling although it might be relatively weak. In contrast, the stimulation of P2Y$_2$ or P2Y$_{12}$ receptor induced a persistent activation of I_{GIRK} (Fig. 7a), indicating that little membrane PIP$_2$ was consumed and resultantly implicating that these two receptors are mainly coupled to G$_{i/o}$ protein. Bodor and colleagues have found that purified P2Y$_{12}$ receptor can form a functional receptor when reconstituted with G$_i$ protein, but not when reconstituted with G$_q$ protein [6]. This is consistent with the present finding that the P2Y$_{12}$ receptor is coupled to G$_{i/o}$ protein to activate I_{GIRK}. In addition, the decay I_{GIRK} evoked by the stimulation of P2Y$_2$ was relatively rapid in comparison to the P2Y$_{12}$, suggesting that some amount of membrane PIP$_2$ was still consumed during the stimulation of P2Y$_2$ and resultantly implicating that P2Y$_2$ is also weakly coupled to G$_q$ protein. The P2Y$_2$ receptor is generally classified to the (PTX-resistant) G$_q$-coupled subfamily [9, 19, 41]. However, the data in the present study suggested that P2Y$_2$ is also coupled to G$_{i/o}$ protein as suggested by other researchers [37], though they

believed that $P2Y_2$ receptor primarily mediates its function through coupling to G_q. Furthermore, these data are also supported by the fact that $P2Y_2$ receptor is sensitive to PTX in stable expressed astrocytoma cells [33] and in human erythroleukemia cells [2].

There is an abundant expression of $P2Y_2$ mRNA in both human atria and ventricles, whereas the mRNA level of $P2Y_2$ is lower than that of $P2Y_1$ or $P2Y_4$ in mouse cardiomyocytes [43]. Musa and colleagues [30] have also indicated that the $P2Y_2$ mRNA level is the most abundant of the eight P2Y receptors in the human right atrium, but is lower than $P2Y_1$ in human sinoatrial node (SAN). They also found that the distribution of P2Y receptor subtypes in rat right atrium, left ventricle, and SAN is quite different with those in the human heart. These results indicate that the P2Y receptor expression varies greatly in the heart, implicating that responses to the stimulation of P2Y receptor are also diverse in different types of cardiac cells. The current study may contribute to understanding the precise regulatory mechanisms underlying the cardiac signaling pathway mediated by P2Y receptors.

References

1. Abbracchio MP, Burnstock G, Boeynaems JM, Barnard EA, Boyer JL, Kennedy C, Knight GE, Fumagalli M, Gachet C, Jacobson KA, Weisman GA (2006) International Union of Pharmacology LVIII: update on the P2Y G protein-coupled nucleotide receptors: from molecular mechanisms and pathophysiology to therapy. Pharmacol Rev 58:281–341
2. Baltensperger K, Porzig H (1997) The P_{2U} purinoceptor obligatorily engages the heterotrimeric G protein G_{16} to mobilize intracellular Ca^{2+} in human erythroleukemia cells. J Biol Chem 272:10151–10159
3. Banfi C, Ferrario S, De Vincenti O, Ceruti S, Fumagalli M, Mazzola A, D'Ambrosi N, Volonte C, Fratto P, Vitali E, Burnstock G, Beltrami E, Parolari A, Polvani G, Biglioli P, Tremoi E, Abbracchio MP (2005) P2 receptors in human heart: upregulation of P2X6 in patients undergoing heart transplantation, interaction with TNFalpha and potential role in myocardial cell death. J Mol Cell Cardiol 39:929–939
4. Bernstein LS, Ramineni S, Hague C, Cladman W, Chidiac P, Levey AL, Hepler JR (2004) RGS2 binds directly and selectively to the M1 muscarinic acetylcholine receptor third intracellular loop to modulate Gq/11alpha signaling. J Biol Chem 279:21248–21256
5. Birnbaumer L (2007) Expansion of signal transduction by G proteins. The second 15 years or so: from 3 to 16 α subunits plus $\beta\gamma$ dimmers. Biochim Biophys Acta 1768:772–793
6. Bodor ET, Waldo GL, Hooks SB, Corbitt J, Boyer JL, Harden TK (2003) Purification and functional reconstitution of the human $P2Y_{12}$ receptor. Mol Pharmacol 64:1210–1216
7. Cho H, Lee D, Lee SH, Ho WK (2005) Receptor-induced depletion of phosphatidylinositol 4,5-bisphosphate inhibits inwardly rectifying K^+ channels in a receptor-specific manner. Proc Natl Acad Sci USA 102:4643–4648
8. Docherty JR (2010) Subtypes of functional alpha1-adrenoceptor. Cell Mol Life Sci 67:405–417
9. Erb L, Liao Z, Seye CI, Weisman GA (2006) P2 receptors: intracellular signaling. Pflugers Arch 452:552–562
10. Erlinge D, Burnstock G (2008) P2 receptors in cardiovascular regulation and disease. Purinergic Signalling 4:1–20
11. Falkenburger BH, Jensen JB, Hille B (2010) Kinetics of PIP2 metabolism and KCNQ2/3 channel regulation studied with a voltage-sensitive phosphatase in living cells. J Gen Physiol 135:99–114
12. Filippov AK, Fernandez-Fernandez JM, Marsh SJ, Simon J, Barnard EA, Brown DA (2004) Activation and inhibition of neuronal G protein-gated inwardly rectifying K(+) channels by P2Y nucleotide receptors. Mol Pharmacol 66:468–477
13. Friel DD, Bean BP (1990) Dual control by ATP and acetylcholine of inwardly rectifying K^+ channels in bovine atrial cells. Pflugers Arch 415:651–657
14. Hara Y, Nakaya H (1997) Dual effects of extracellular ATP on the muscarinic acetylcholine receptor-operated K^+ current in guinea-pig atrial cells. Eur J Pharmacol 324:295–303
15. Hill JJ, Peralta EG (2001) Inhibition of a G_i-activated potassium channel (GIRK1/4) by the G_q-coupled m1 muscarinic acetylcholine receptor. J Biol Chem 276:5505–5510
16. Hwang TC, Horie M, Nairn AC, Gadsby DC (1992) Role of GTP-binding proteins in the regulation of mammalian cardiac chloride conductance. J Gen Physiol 99:465–489
17. Keselman I, Fribourg M, Felsenfeld DP, Logothetis DE (2007) Mechanism of PLC-mediated Kir3 current inhibition. Channels (Austin) 1:113–123
18. Kobrinsky E, Mirshahi T, Zhang H, Jin T, Logothetis DE (2000) Receptor-mediated hydrolysis of plasma membrane messenger PIP2 leads to K^+-current desensitization. Nat Cell Biol 2:507–514
19. Koles L, Gerevich Z, Oliveira JF, Zadori ZS, Wirkner K, Illes P (2008) Interaction of P2 purinergic receptors with cellular macromolecules. Naunyn-Schmiedeberg's Arch Pharmacol 377:1–33
20. Krapivinsky G, Gordon EA, Wickman K, Velimirovic B, Krapivinsky L, Clapham DE (1995) The G-protein-gated atrial K^+ channel I_{KACh} is a heteromultimer of two inwardly rectifying K^+-channel proteins. Nature 374:135–141
21. Kurachi Y, Nakajima T, Sugimoto T (1986) On the mechanism of activation of muscarinic K^+ channels by adenosine in isolated atrial cells: involvement of GTP-binding proteins. Pflugers Arch 407:264–274
22. Leaney JL, Dekker LV, Tinker A (2001) Regulation of a G protein-gated inwardly rectifying K^+ channel by a Ca^{2+}-independent protein kinase C. J Physiol 534:367–379
23. Mao J, Wang X, Chen F, Wang R, Rojas A, Shi Y, Piao H, Jiang C (2004) Molecular basis for the inhibition of G protein-coupled inward rectifier K^+ channels by protein kinase C. Proc Natl Acad Sci USA 101:1087–1092
24. Matsuura H, Sakaguchi M, Tsuruhara Y, Ehara T (1996) Activation of the muscarinic K^+ channel by P_2-purinoceptors via pertussis toxin-sensitive G proteins in guinea-pig atrial cells. J Physiol 490:659–671

25. Matsuura H, Ehara T (1996) Modulation of the muscarinic K$^+$ channel by P$_2$-purinoceptors in guinea-pig atrial myocytes. J Physiol 497:379–393

26. Matsuura H, Ehara T (1992) Activation of chloride current by purinergic stimulation in guinea pig heart cells. Circ Res 70:851–855

27. Matsuura H, Ehara T (1997) Selective enhancement of the slow component of delayed rectified K$^+$ current in guinea-pig atrial cells by external ATP. J Physiol 503:45–54

28. Matsuura H, Tsuruara Y, Sakaguchi M, Ehara T (1996) Enhancement of delayed rectifier K$^+$ current by P$_2$-purinoceptor stimulation in guinea-pig atrial. J Physiol 490:647–658

29. Meyer T, Wellner-Kienitz MC, Biewald A, Bender K, Eickel A, PottlT L (2001) Depletion of phosphatidylinositol 4,5-bisphosphate by activation of phospholipase C-coupled receptors causes slow inhibition but not desensitization of G protein-gated inward rectifier K$^+$ current in atrial myocytes. J Biol Chem 276:5650–5658

30. Musa H, Tellez JO, Chandler NJ, Greener ID, Maczewski M, Mackiewicz U, Beresewicz A, Molenaar P, Boyett MR, Dobrzynski H (2009) P2 purinergic receptor mRNA in rat and human sinoatrial node and other heart regions. Naunyn Schmiedebergs Arch Pharmacol 379:541–549

31. Neitzel KL, Hepler JR (2006) Cellular mechanisms that determine selective RGS protein regulation of G protein-coupled receptor signaling. Semin Cell Dev Biol 17:383–389

32. Nikolov EN, Ivanova-Nikolova TT (2004) Coordination of membrane excitability through a GIRK1 signaling complex in the atria. J Biol Chem 279:23630–23636

33. Parr CE, Sullivan DM, Paradiso AM, Lazarowski ER, Burch LH, Olsen JC, Erb L, Weisman GA, Boucher RC, Turner JT (1994) Cloning and expression of a human P$_{2U}$ nucleotide receptor, a target for cystic fibrosis pharmacotherapy. Proc Natl Acad Sci USA 91:3275–3279

34. Pfaffinger PJ, Martin JM, Hunter DD, Nathanson NM, Hille B (1985) GTP-binding proteins couple cardiac muscarinic receptors to a K channel. Nature 317:536–538

35. Soejima M, Noma A (1984) Mode of regulation of the ACh-sensitive K-channel by the muscarinic receptor in rabbit atrial cells. Pflugers Arch 400:424–431

36. Stevens EB, Shah BS, Pinnock RD, Lee K (1999) Bombesin receptors inhibit G protein-coupled inwardly rectifying K$^+$ channels expressed in *Xenopus* oocytes through a protein kinase C-dependent pathway. Mol Pharmacol 55:1020–1027

37. Talasila A, Germack R, Dickenson JM (2009) Characterization of P2Y receptor subtypes functionally expressed on neonatal rat cardiac myofibroblasts. Br J Pharmacol 58:339–353

38. Thaning P, Bune LT, Hellsten Y, Pilegaard H, Saltin B, Rosenmeier JB (2010) Attenuated purinergic receptor function in patients with type 2 diabetes. Diabetes 59:182–189

39. Tsang S, Woo AY, Zhu W, Xiao RP (2010) Deregulation of RGS2 in cardiovascular diseases. Front Biosci (Schol Ed) 2:547–557

40. Vassort G (2001) Adenosine 5′-triphosphate: a P2-purinergic agonist in the myocardium. Physiol Rev 81:767–806

41. Von Kugelgen I (2006) Pharmacological profiles of cloned mammalian P2Y-receptor subtypes. Pharmacol Ther 110:415–432

42. Waldo GL, Harden TK (2004) Agonist binding and Gq-stimulating activities of the purified human P2Y$_1$ receptor. Mol Pharmacol 65:426–436

43. Wihlborg AK, Balogh J, Wang L, Borna C, Dou Y, Joshi BV, Lazarowski E, Jacobson KA, Amer A, Erlinge D (2006) Positive inotropic effects by uridine triphosphate (UTP) and uridine diphosphate (UDP) via P2Y$_2$ and P2Y$_6$ receptors on cardiomyocytes and release of UTP in man during myocardial infarction. Circ Res 98:970–976

44. Yasuda Y, Matsuura H, Ito M, Matsumoto T, Ding WG, Horie M (2005) Regulation of the muscarinic K$^+$ channel by extracellular ATP through membrane phosphatidylinositol 4,5-bisphosphate in guinea-pig atrial myocytes. Br J Pharmacol 145:156–165

A Connexin40 Mutation Associated With a Malignant Variant of Progressive Familial Heart Block Type I

Naomasa Makita, MD, PhD; Akiko Seki, MD, PhD; Naokata Sumitomo, MD, PhD;
Halina Chkourko, MS; Shigetomo Fukuhara, PhD; Hiroshi Watanabe, MD, PhD;
Wataru Shimizu, MD, PhD; Connie R. Bezzina, PhD; Can Hasdemir, MD; Hideo Mugishima, MD;
Takeru Makiyama, MD, PhD; Alban Baruteau, MD; Estelle Baron, BS; Minoru Horie, MD, PhD;
Nobuhisa Hagiwara, MD, PhD; Arthur A.M. Wilde, MD; Vincent Probst, MD, PhD;
Hervé Le Marec, MD; Dan M. Roden, MD; Naoki Mochizuki, MD, PhD;
Jean-Jacques Schott, PhD; Mario Delmar, MD, PhD

Background—Progressive familial heart block type I (PFHBI) is a hereditary arrhythmia characterized by progressive conduction disturbances in the His-Purkinje system. PFHBI has been linked to genes such as *SCN5A* that influence cardiac excitability but not to genes that influence cell-to-cell communication. Our goal was to explore whether nucleotide substitutions in genes coding for connexin proteins would associate with clinical cases of PFHBI and if so, to establish a genotype-cell phenotype correlation for that mutation.

Methods and Results—We screened 156 probands with PFHBI. In addition to 12 sodium channel mutations, we found a germ line *GJA5* (connexin40 [Cx40]) mutation (Q58L) in 1 family. Heterologous expression of Cx40-Q58L in connexin-deficient neuroblastoma cells resulted in marked reduction of junctional conductance (Cx40-wild type [WT], 22.2 ± 1.7 nS, n=14; Cx40-Q58L, 0.56 ± 0.34 nS, n=14; $P<0.001$) and diffuse localization of immunoreactive proteins in the vicinity of the plasma membrane without formation of gap junctions. Heteromeric cotransfection of Cx40-WT and Cx40-Q58L resulted in homogenous distribution of proteins in the plasma membrane rather than in membrane plaques in $\approx 50\%$ of cells; well-defined gap junctions were observed in other cells. Junctional conductance values correlated with the distribution of gap junction plaques.

Conclusions—Mutation Cx40-Q58L impairs gap junction formation at cell-cell interfaces. This is the first demonstration of a germ line mutation in a connexin gene that associates with inherited ventricular arrhythmias and emphasizes the importance of Cx40 in normal propagation in the specialized conduction system. (***Circ Arrhythm Electrophysiol.* 2012; 5:163-172.)**

Key Words: heart block ■ genes ■ ion channels ■ death sudden ■ gap junctions

Cardiac myocyte excitability in atria, His-Purkinje system, and ventricles is largely determined by the properties of voltage-gated sodium channels. Once activated, excitatory currents rapidly propagate to neighboring cells through low-resistance intercellular channels called gap junctions, which facilitate the synchronous contraction of the heart.[1,2] Loss of expression and function of cardiac gap junctions and sodium currents can severely impair action potential propagation, which sets the stage for life-threatening arrhythmias.[1,2] Although multiple mutations in genes coding for components of the voltage-gated sodium channel complex have been previ-

Clinical Perspective on p 172

ously described in relation to arrhythmias and sudden death in young persons[3] and connexin40 (Cx40) mutations have been implicated in atrial fibrillation,[4,5] no study has identified an

association between germ line mutations in gap junction proteins and inherited ventricular arrhythmias in humans.

In this study, we investigated a group of patients with progressive familial heart block type I (PFHBI) (Online Mendelian Inheritance in Man 113900), also known as progressive cardiac conduction defect or Lenègre-Lev disease,[6,7] is a dominant inherited disorder of the His-Purkinje system. Affected individuals show electrocardiographic evidence of bundle branch disease (ie, right bundle branch block, left anterior or posterior hemiblock, complete heart block) with broad QRS complexes. The disease can progress from a normal ECG to right bundle branch block and from the latter to complete heart block. Affected individuals often present with family history of syncope, pacemaker implantation, and sudden death.[8] Although structural abnormalities have been invoked as a cause of the disease,[6,7] a number of patients present with normal cardiac structure and contractile function. Linkage analysis in a large South African PFHBI kindred[9] and a Lebanese kindred[10] mapped a causal locus on chromosome 19q13.3, and further work identified mutations in genes encoding for the transient receptor potential nonselective cation channel, subfamily M, member 4 (*TRPM4*) gene[11] at this locus. Haploinsufficiency of *SCN5A* and aging have been implicated in PFHBI,[8] and age-dependent manifestations of the disease have been recapitulated in mice.[12]

Here, we sought to expand on the association between PFHBI and mutations in genes relevant to action potential propagation; in particular, we assessed the possible association between nucleotide substitutions in connexin-coding genes and PFHBI. We evaluated 156 probands of diverse ethnic backgrounds from Asia, Europe, and North America given a clinical diagnosis of PFHBI. In addition to the sodium channel mutations previously reported,[13–15] we identified a germ line missense mutation in *GJA5* in a family with severe, early onset disease. This gene codes for the gap junction protein connexin40 (Cx40), which predominantly expresses in the atria and His-Purkinje system.[16] Heterologous expression experiments revealed that this novel mutation (Cx40-Q58L) significantly impaired the ability of Cx40 to form gap junction channels. Confocal microscopy showed that the Cx40-Q58L mutant but not the wild type (WT) failed to form plaques at sites of cell-cell apposition. Coexpression experiments indicated that the Cx40-WT protein provided only partial rescue of the Cx40-Q58L cellular phenotype. To our knowledge, this is the first description of a germ line mutation in a connexin gene associated with inherited ventricular arrhythmias. The results open the possibility of *GJA5* as a candidate gene for screening in patients with PFHB1, yet in the absence of further evidence, screening may be limited to the research environment rather than included as a part of the routine diagnostic examination.[17] The data also emphasize the importance of Cx40 in the maintenance of normal propagation in the specialized conduction system of the human heart.

Methods

Genetic Screening of PFHB1

Genomic screening by polymerase chain reaction and DNA sequencing was performed for *GJA5* (Cx40), *GJA1* (Cx43), *GJC1* (Cx45), *KCNQ1, KCNH2, SCN5A, KCNE1, KCNE2, KCNJ2, SCN1B,*

SCN4B, HCN4. Primer information is provided in the online-only Data Supplement. All participating probands and family members gave written informed consent in accordance with standards (Declaration of Helsinki) and local ethics committees.

Plasmid Construction

A 1.1-kb Cx40-DNA fragment was subcloned into bicystronic plasmids pIRES2-EGFP and pIRES2-DsRED2. An EGFP or FLAG epitope was added at Cx40 C terminal to generate EGFP- or FLAG-tagged Cx40. Site-directed mutagenesis (Q58L) was performed with QuikChange. Primer information and additional details are provided in the online-only Data Supplement.

Cell Culture and Transfection

Constructs were introduced into connexin-deficient HeLa cells or mouse neuroblastoma (N2A) cells using Lipofectamine as per manufacturer's protocol.

Electrophysiology

Gap junction currents were recorded from transiently transfected N2A cell pairs using whole-cell double-patch clamp techniques as previously described.[18,19] Further details are provided in the online-only Data Supplement.

Immunocytochemistry and Western Blotting

HeLa cells, transfected with pEGFPN1-Cx40-WT, pCMV-FLAG-Cx40-Q58L, or both, were stained with anti-FLAG M2 antibody and Alexa546-labeled secondary antibody. EGFP and Alexa546 fluorescence images were recorded by confocal microscopy. For western blotting, N2A cells were transiently transfected with 3 μg of Cx40 plasmids. Two days after transfection, cells were lysed, and proteins were extracted and separated by conventional methods. Further details are provided in the online-only Data Supplement.

Statistical Analysis

Results are presented as mean$\pm$SEM. Mann-Whitney rank sum tests with Bonferroni post hoc correction were used in comparisons for which normality or equal variance assumptions were invalid. In other instances, differences between groups were assessed by 1-way ANOVA followed by Bonferroni post hoc correction. Statistical significance was assumed for $P<0.05$.

Results

Genetic Screening of PFHBI Probands

We genetically screened 156 probands given a clinical diagnosis of PFHBI. We identified 4 novel and 5 previously reported mutations in *SCN5A*,[13,15] 3 mutations in *SCN1B*,[14] and a novel germ line heterozygous missense mutation in exon 2 of the Cx40 gene *GJA5* (online-only Data Supplement Table I). Mutations were not found in connexin genes *GJA1* (Cx43) or *GJC1* (Cx45) or in the other genes screened (*KCNQ1, KCNH2, KCNE1, KCNE2, KCNJ2, HCN4,* or *SCN4B*). Of the novel *SCN5A* mutations, 1 caused a modification of the amplitude and voltage gating kinetics of the sodium current in heterologously expressing cells (online-only Data Supplement Figure I); 3 other mutant constructs failed to express functional channels, suggesting that patients carrying the mutation were functionally haploinsufficient for Nav1.5 (online-only Data Supplement Figure I). The *GJA5* mutation (c.173A>T) caused an amino acid substitution (glutamine [Q] replaced by leucine [L]) at position 58 in Cx40 (Cx40-Q58L) (Figure 1A and 1B). The mutation was absent in 400 alleles from unaffected control subjects and in the other 155 PFHBI probands. Screening of the entire gene
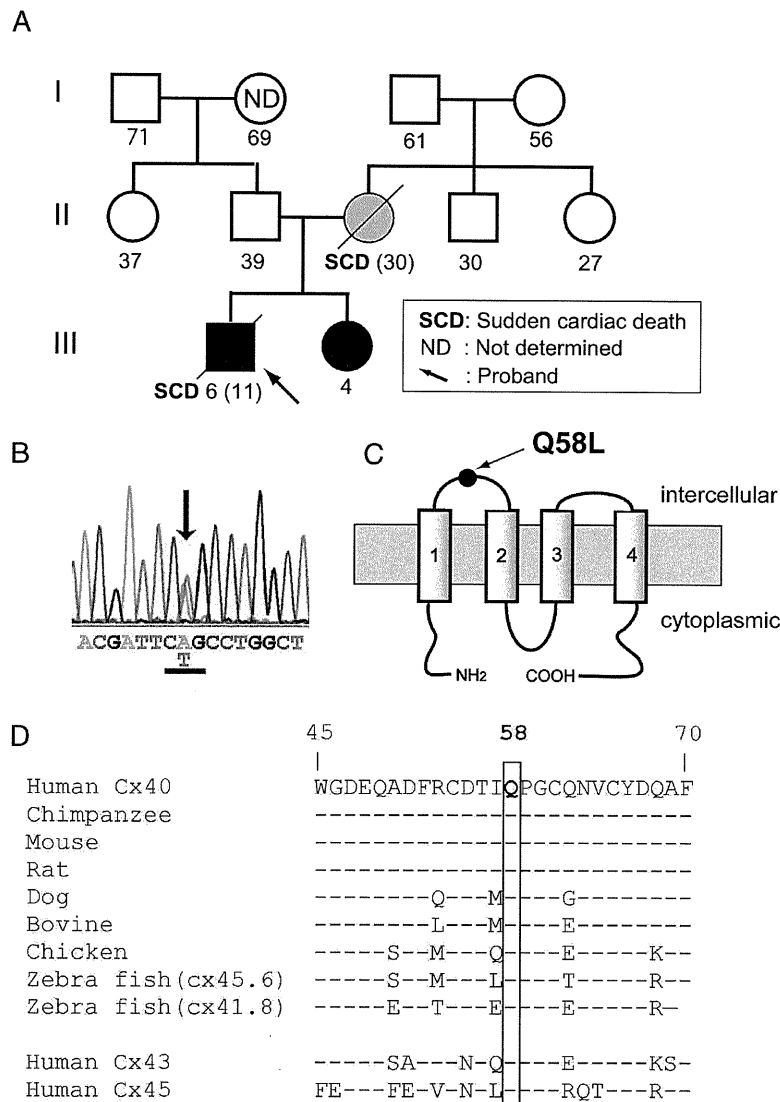
A

B

C   Q58L

D

	45	58	70

```
                       45            58          70
                       |             |           |
Human  Cx40            WGDEQADFRCDTIQPGCQNVCYDQAF
Chimpanzee             -------------|-|-----------
Mouse                  -------------|-|-----------
Rat                    -------------|-|-----------
Dog                    --------Q---M|-|--G--------
Bovine                 --------L---M|-|--E--------
Chicken                -----S--M---Q|-|--E-----K--
Zebra fish(cx45.6)     -----S--M---L|-|--T-----R--
Zebra fish(cx41.8)     -----E--T---E|-|--E-----R--

Human  Cx43            -----SA---N-Q|-|--E-----KS-
Human  Cx45            FE---FE-V-N-L|-|--RQT---R--
```

Figure 1. *GJA5* mutation identified in a family given the clinical diagnosis of progressive familial heart block type I. **A,** Family pedigree. Genetically affected and unaffected individuals are shown with closed and open symbols, respectively. The hatched circle indicates the proband's mother not genotyped; clinical data suggest that she was a de novo mutation carrier. Number below each symbol indicates the age at registration or age of SCD (parenthesis). **B,** Sequence electropherogram of exon 2 *GJA5* of proband. Arrow indicates heterozygous missense mutation of leucine (CTG) for glutamine-58 (CAG). **C,** Cx40 predicted membrane topology indicating position Q58 in first extracellular loop. **D,** Sequence alignment of human Cx40 and its homologues (residues 45–70). Notice the conservation in human Cx43 and Cx45. Dashes indicate residues identical with the top sequence. Cx indicates connexin.

panel (including *SCN5A* and *SCN1B*) revealed no other sequence modification in the DNA of this proband. Topological analysis placed amino acid 58 of Cx40 within the first extracellular loop (Figure 1C). The presence of glutamine in this position is highly conserved among *GJA5* orthologs, and 2 other cardiac connexins, Cx43 and Cx45 (Figure 1D). The clinical and genotypic characteristics of proband and tested family members are described next.

Clinical Phenotypes and Genotype of the PFHBI Pedigree With the *GJA5* Mutation

The proband, an 11-year-old boy at time of death, was first referred for evaluation when he was age 6 years because of ECG abnormalities. Although asymptomatic at that time, his ECG showed advanced atrioventricular block, complete left bundle branch block, and left axis deviation (Figure 2A). Echocardiography and cardiac scintigraphy did not reveal

signs of structural heart disease. He experienced an episode of syncope at age 9; implantation of a permanent pacemaker was recommended by the physician but not authorized by the legal guardian. The proband died suddenly 2 years later during exercise (running), and the family declined postmortem examination. The proband's younger sister shares the Cx40-Q58L mutation. She is asymptomatic, with a QRS duration at the upper limit of normal, left axis deviation that has been progressive (online-only Data Supplement Table II), and QRS notch. These findings are consistent with impaired intraventricular conduction (Figure 2B). The mother died suddenly at age 30 after delivering the second child. An ECG on record, obtained when she was age 16, was similar to that of the proband (compare Figure 2C with 2A). In addition, a ventricular tachycardia was recorded during the recovery phase of an exercise stress test (online-only Data Supplement Figure II). DNA from the mother was not available for
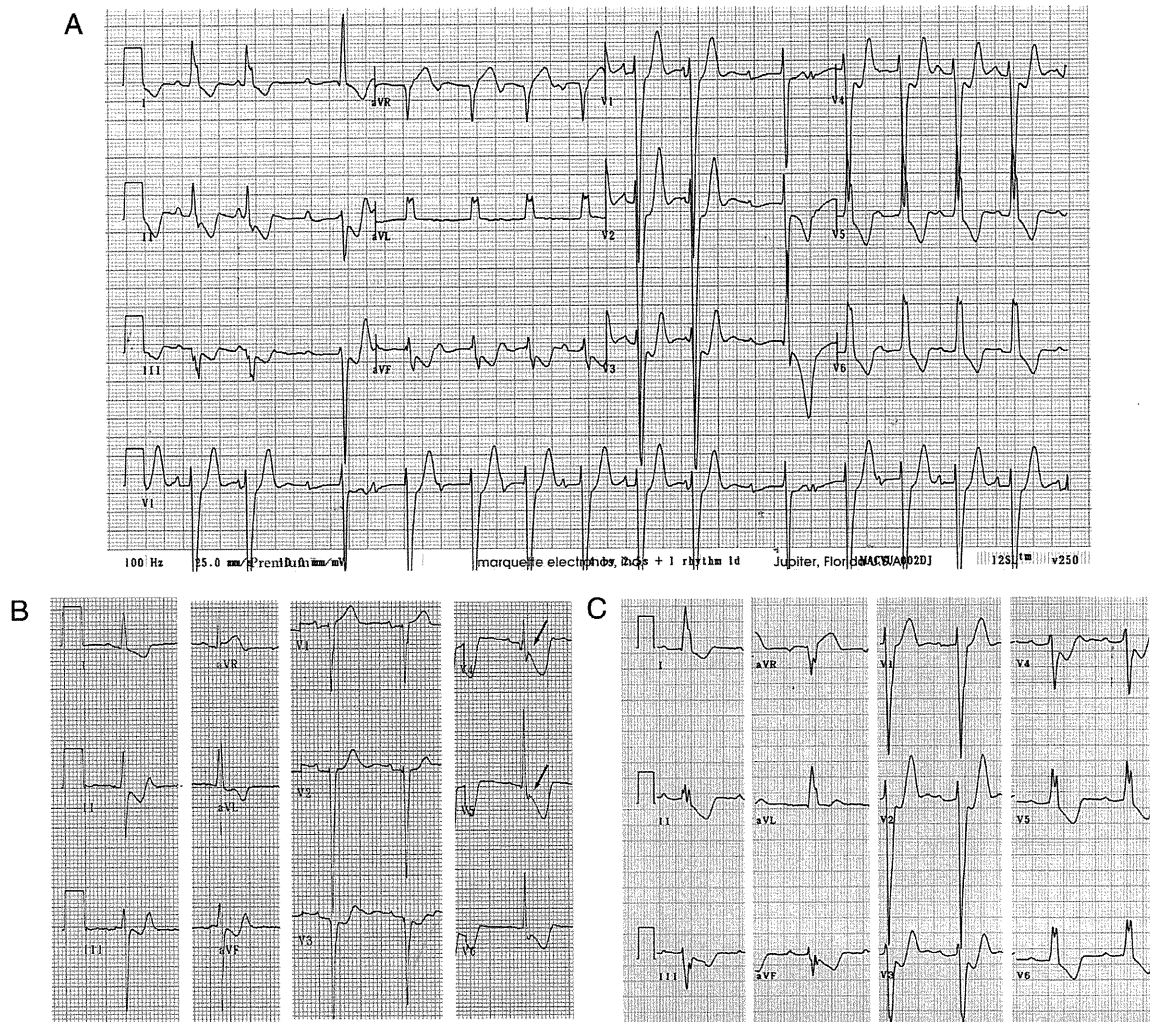
A

B

C

Figure 2. ECGs of proband and affected family members. **A**, ECG of proband at age 6 years, showing advanced atrioventricular block, complete left bundle branch block, and left axis deviation. Patient died suddenly 5 years later. **B**, ECG of proband's sister at age 6 years, showing QRS duration at the upper limit of normal, left axis deviation that has been progressive, and QRS notch in leads V4 and V5 (arrows) consistent with impaired intraventricular conduction. **C**, ECG of proband's mother at age 16 years, showing complete left bundle branch block and left axis deviation. She died suddenly at age 30.

examination. Other family members, including the proband's father, showed normal ECGs. DNA analysis of proband's father and maternal grandparents revealed absence of the Cx40-Q58L mutation. On the basis of clinical data and genotypic features of the proband and sister, it is most likely that the Cx40-Q58L mutation appeared de novo in the proband's mother. The data also indicate an early onset of PFHBI in this family compared with the natural history of the disease in most other cases.[8] As an initial step to assess the functional implications of the Cx40-Q58L mutation, modified constructs were transiently expressed in an exogenous system and evaluated for localization and function.

Electrophysiological Properties of Mutant Cx40-Q58L Channels

Connexin-deficient N2A cells were transiently transfected with cDNA for Cx40-WT or Cx40-Q58L; electrophysiolog-

ical properties of homologous Cx40 channels were analyzed by conventional dual whole-cell patch clamp. Figure 3A shows representative junctional current traces elicited by a transjunctional voltage gradient of -60 mV. Average junctional conductance (Gj) decreased from 22.2 ± 1.7 nS in cells expressing Cx40-WT (n=14) to 0.56 ± 0.34 nS in cells expressing the Cx40-Q58L mutant (n=14; $P < 0.001$). The probability of functional coupling, calculated by dividing the number of electrically coupled pairs by the number of pairs tested, was 100% and 57.1% for Cx40-WT and Cx40-Q58L, respectively.

Figure 3B depicts representative single-channel recordings elicited by a transjunctional voltage of -60 mV in cell pairs expressing Cx40-WT or Cx40-Q58L. Unitary events for WT channels displayed current transitions corresponding to 2 conducting states (O_1 and O_2) of 43.3 and 119.5 pS, respectively. Figure 3C shows the event histograms for both cell
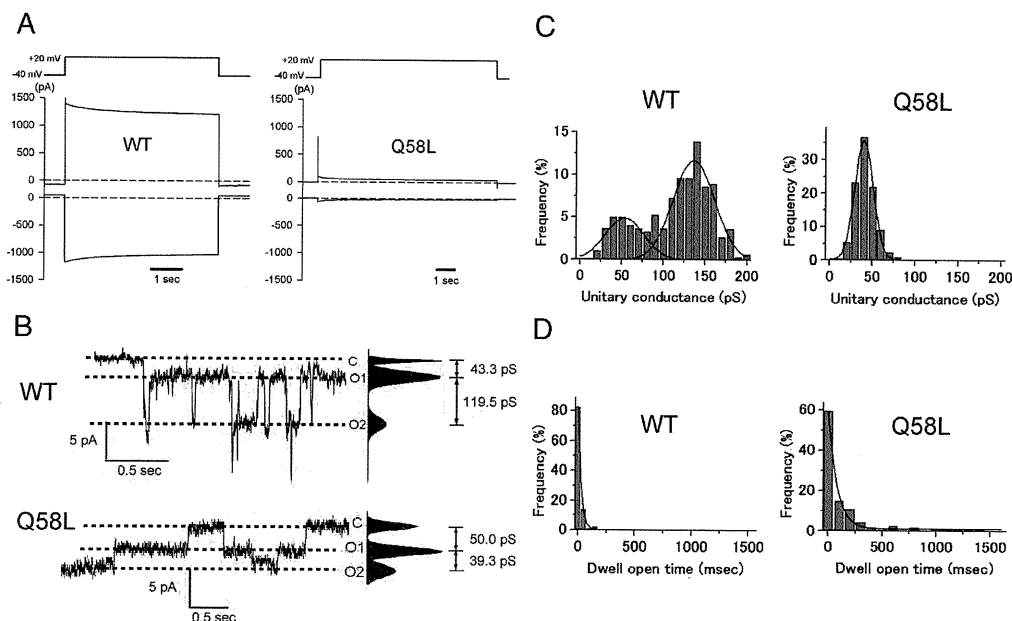
Figure 3. Whole-cell and single-channel properties of connexin40 (Cx40)-WT and Cx40–Q58L channels. A, Voltage pulse (top) and junctional current (bottom) from a homomeric WT cell pair (junctional conductance, 12.9 nS) and a Q58L cell pair (junctional conductance, 1.2 nS). B, Unitary currents recorded from homomeric Cx40-WT and Cx40–Q58L channels. O₁ and O₂ refer to 2 conducting (open) unitary levels of current. C, All-event histograms pooled from WT (n=3) and Q58L (n=3) cells with homologous channels. For WT, Gaussian peaks centered at 136.2±2.3 and 53.1±5.3 pS. For Q58L, best fit by a single Gaussian distribution centered at 40.2±0.3 pS (n=3). D, Frequency of events in relation to dwell open time. Binned data were fit by single exponentials (τ_{open} WT, 27.9±0.5 ms, 4 cells, 186 events; τ_{open} Q58L, 92.0±7.8 ms, 3 cells, 163 events). WT indicates wild type.

types (Cx40-WT, 3 cell pairs and 303 events; Cx40-Q58L, 3 cell pairs and 416 events). The histogram for the Cx40-WT channels was best described by 2 Gaussian distributions centered at 136.2±2.3 and 53.1±5.3 pS. In contrast, the histogram for Cx40-Q58L channels was best described by a single Gaussian function centered at 40.2±0.3 pS. Moreover, the length of time that a channel dwelled in the open state (dwell open time) was substantially longer for the Cx40-Q58L channels (92.0±7.8 ms, 3 cell pairs, 163 events) than for Cx40-WT channels (27.9±0.5 ms, 4 cell pairs, and 186 events) (Figure 3D). Of note, the Q58L mutation had a strong dominant effect on formation of heterotypic functional gap junctions. Cells were transfected with either pIRES2-EGFP-Cx40-WT or pIRES2-DsRED2-Cx40-Q58L, and heterotypic pairs were identified by fluorescence microscopy (an EGFP-expressing cell paired with a DsRED2-expressing cell). We recorded from 8 cell pairs and detected unitary current events in only 2 pairs. A total of 57 events were recorded, and average macroscopic junctional conductance was 0.04±0.03 nS. Collectively, the data demonstrated that the Q58L mutation significantly affects the biophysical properties of Cx40 channels and the overall ability of Cx40 gap junctions to form a low-resistance pathway between cells.

Electrophysiological Properties and Gap Junction Plaque Formation in Cells Coexpressing WT and Q58L Proteins

In the clinical cases identified, the Q58L mutation was detected in only 1 carrier allele. Therefore, we assessed the function of gap junctions in cells coexpressing WT and mutant proteins. N2A cells were cotransfected with cDNA for both GFP-tagged Cx40-WT and Cx40-Q58L (0.5 µg of pEGFPN1-Cx40-WT combined with 0.5 µg of pEGFPN1-Cx40-Q58L). Results were compared with those obtained when only 1 of the constructs (1 µg) was transfected. Cells expressing both constructs (WT/Q58L) showed intermediate conductance (15.4±3.7 nS, n=16) between WT (28.8±3.6 nS, n=16, P<0.001) and Q58L (0.28±0.11 nS, n=14, P<0.001) (Figure 4A). These values were comparable to those obtained using the bicistronic pIRES2-EGFP constructs (WT, 22.2±1.7 nS, n=14; WT/Q58L, 13.0±2.4 nS, n=17; Q58L, 0.56±0.34 nS, n=14). The coexpression results were consistent with those obtained using pIRES plasmids that tagged the cells both green and red, if cotransfected (online-only Data Supplement Figure I). The probability of finding functional coupling in cotransfected cells was 76.5%, which was intermediately between WT (100%) and Q58L (57.1%).

The characteristics of gap junction plaques observed in cells coexpressing WT and Q58L varied significantly between pairs (Figure 4B). Nearly one half of transfected (fluorescence-positive) cells exhibited clear and discrete gap junction plaques (arrow a), whereas the rest of fluorescent-positive cells showed a diffuse expression pattern and absence of well-defined plaques (arrow b). Fluorescence-positive and gap junction plaque-positive cells were counted in 10 different views for each group, and efficacy of gap junction plaque formation was statistically analyzed (Figure 4C) by calculating the ratio of cells with gap junction plaques